# Lunar meteorite Northwest Africa 11962: A regolith breccia containing various examples of titanium-rich lunar volcanism and the high alkali suite.

Journal Item

The Meteoritical Society

*Meteoritics & Planetary Science* 1–21 (2021)
doi: 10.1111/maps.13659

# Lunar meteorite Northwest Africa 11962: A regolith breccia containing records of titanium-rich lunar volcanism and the high alkali suite

Andreas BECHTOLD[1]*, Franz BRANDSTÄTTER[2], Lidia PITTARELLO[2], Ludovic FERRIÈRE[2], Richard C. GREENWOOD[3], and Christian KOEBERL[1]

[1]Department of Lithospheric Research, University of Vienna, Althanstrasse 14, Vienna 1090, Austria
[2]Natural History Museum Vienna, Burgring 7, Vienna 1010, Austria
[3]Planetary and Space Sciences, School of Physical Sciences, The Open University, Walton Hall, Milton Keynes MK7 6AA, UK
*Corresponding author. E-mail: andreas.bechtold@univie.ac.at

*(Received 02 October 2020; revision accepted 03 April 2021)*

**Abstract**–Northwest Africa (NWA) 11962 is a lunar regolith breccia composed of a wide range of different clasts. The lunar origin of this meteorite is confirmed by oxygen isotope analysis and the Fe/Mn ratio in pyroxene and olivine. In the present study, the clasts and the matrix of NWA 11962 are characterized by optical and electron microscopy along with electron microprobe analyses and micro-Raman spectroscopy. The meteorite has a glassy impact melt matrix, which accounts for 35% of the surface area in the two thin sections examined, and which contains a very large variety of different lithic clasts, monomineralic clasts, and glass fragments. The presence of volcanic and impact-related glass spherules led to the classification of this meteorite as a regolith breccia. Lithic clasts include numerous fragments of quartz monzogabbro and lunar felsite, which are quite rare lithologies in the lunar alkali suite. However, the most abundant components in the breccia are gabbroic clasts. The mineral chemistry of the pyroxenes in the gabbroic clasts and the chemistry of various types of glass fragments in the breccia indicate an origin of the regolith from an area with low-Ti to high-Ti mare basalt volcanism. In addition to the peculiar petrographic characteristics of NWA 11962, the possible pairing relationships with other lunar meteorites are discussed.

## INTRODUCTION

The number of recognized lunar meteorites, rocks that were ejected from the Moon by impact and have subsequently fallen on Earth, increases every year, contributing to an improvement in our knowledge of the geological past of the Moon (e.g., Warren 1998; Korotev 2005; Joy and Arai 2013; Gross et al. 2014; Stephant et al. 2019). Lunar meteorites are randomly sampled from virtually the entire lunar surface, in contrast to the Apollo and Luna samples that were collected from a relatively limited area. Therefore, lunar meteorites have been used to calibrate lunar surface concentration data for several elements obtained by orbital missions. These data have subsequently been used as basis for estimates of the chemical composition of the lunar crust and the bulk Moon (Warren 2005). A more specific example of the lessons that have been learned from lunar meteorites is the realization that the so-called Mg-suite (Mg-rich) of lunar rocks is poorly represented in the lunar highlands, something that was not clear from the study of the Apollo samples (Neal [2009] and references therein). As of March 20, 2021, the Meteoritical Bulletin Database lists 439 lunar meteorites (i.e., with a different name), representing a total mass of ~692 kg, which exceeds the total mass returned from Apollo (~382 kg), Luna (~301 g), and Chang'e 5 (1.7 kg) missions. However, it is not entirely clear how many of these "different" lunar meteorites belong to the same impact ejection event and are thus launch-paired stones (e.g., Day et al. 2006; Valencia et al. 2019). This question is important because, as mentioned above, they contribute to a better understanding of the lunar geology, and, therefore, it is

of value to know how many "individual collection points" on the crust they represent. In a recent review publication, Korotev and Irving (2021) estimate that for the ~341 lunar meteorites for which data are available, they represent 109–134 different lunar launch sites. A certain number of lunar meteorites are so-called regolith breccias, made up of consolidated lunar regolith. Regolith is the planetary surface layer made of unconsolidated rock fragments or debris overlaying the bedrock, known from many solid planetary bodies like asteroids or Mars. The individual components of lunar regolith breccias provide a good overview of the geology, and therefore, the composition of the local crust from which they originate. For this reason, we report here on the petrography of the recently confirmed meteorite NWA 11962, a lunar regolith breccia, and discuss its possible pairing relations to other known lunar meteorites.

## ANALYTICAL METHODS

The specimens investigated in this work derive from the main mass of NWA 11962, from the meteorite collection of the Natural History Museum (NHM) Vienna, Austria (Figs. 1a and 1b). Two petrographic polished thin sections (ca. 30 μm thickness) were prepared for optical and scanning electron microscopy, denoted as NHMV-O266 (Figs. 1c and 1d) and NHMV-O267 (Figs. 1e and 1f). The oxygen stable-isotopic composition was measured at the Open University, Milton Keynes (UK), using the technique described in Greenwood et al. (2014, 2017).

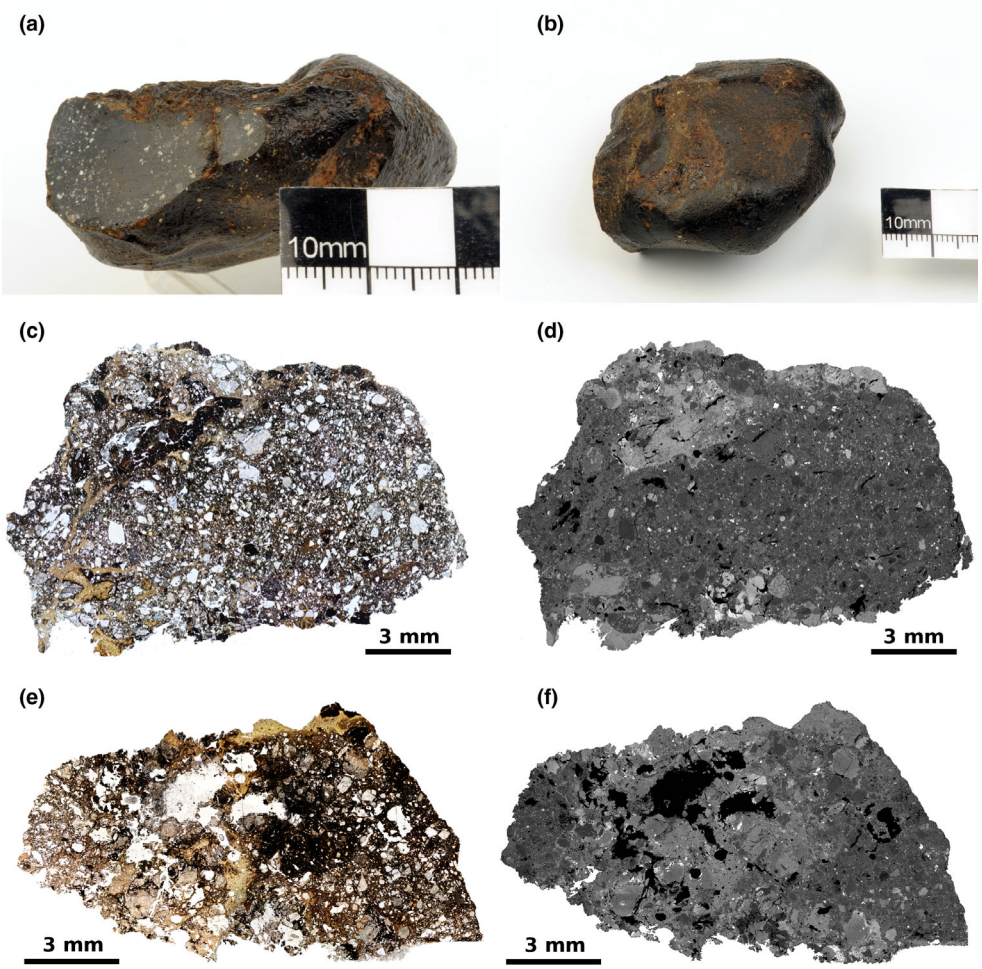


Fig. 1. Lunar meteorite Northwest Africa 11962. a, b) Macrophotos of the meteorite. Credit Alice Schumacher, NHM Vienna. c) Thin section NHMV-O266 in plane-polarized light (PPL). d) Backscattered electron (BSE) mosaic image of thin section NHMV-O266. e) Thin section NHMV-O267 in PPL. f) BSE mosaic image of thin section NHMV-O267. The BSE mosaic images (on the right side, d and f) show contrasting areas of gabbroic clasts and related melt and fragments (bright areas) and areas of mainly alkali- and Mg-suite material (dark areas). The black areas in the BSE mosaic images are cavities in the rock, as well as areas where material was lost during thin section preparation.

### Petrography and Mineral Chemistry

After optical microscopy, the thin sections were carbon-coated and examined using a JEOL JSM 6610-LV scanning electron microscope (SEM) at the NHM Vienna. Operating conditions were 15 kV accelerating voltage and a beam current of 1.2 nA. Images were collected in backscattered electron mode (BSE) and were used for image analysis, using the software JMicroVision (Roduit 2020). Quantitative analyses of mineral compositions were obtained with a JEOL JXA 8530-F field emission electron microprobe (EPMA) at the NHM Vienna and a CAMECA SX Five field emission electron microprobe at the Department of Lithospheric Research, University of Vienna. Both instruments are equipped with five wavelength dispersive spectrometers and an energy dispersive spectrometer. The compositions of minerals were obtained at 15 kV accelerating voltage and a beam current of 20 nA with a spot size of 1 μm for mafic phases and a defocused beam for glasses and felsic phases. Natural and synthetic reference materials were used for calibration. With the JEOL JXA 8530-F microprobe, the maximum detection limit in the silicate phases and glasses measured was 195 ppm (Si), 153 ppm (Al), 442 ppm (Fe), 133 ppm (Mg), 100 ppm (Ca), 117 ppm (Na), 375 ppm (Mn), 214 ppm (Ti), and 73 ppm (K). With the CAMECA SX Five microprobe, the maximum detection limit in the silicate phases and glasses measured was 348 ppm (Si), 281 ppm (Al), 882 ppm (Fe), 334 ppm (Mg), 436 ppm (Ca), 318 ppm (Na), 565 ppm (Mn), 325 ppm (Ti), and 430 ppm (K). Additional details on the microprobe detection limits can be found in the supplementary information (Table S1).

In addition, to characterize the different silica polymorphs, Raman spectra were obtained with a Renishaw RM1000 confocal edge filter-based micro-Raman spectrometer with a 20 mW, 488 nm Argon ion laser excitation system, a grating with 1200 lines $mm^{-1}$, and a thermoelectrically cooled CCD array detector at the Institute of Mineralogy and Crystallography, University of Vienna. Spectra were obtained in the range from 48 to 1663 $cm^{-1}$, with 300 s acquisition time. The spectral resolution of the system (apparatus function) was 5–6 $cm^{-1}$ and the wave number accuracy was better than $\pm 1$ $cm^{-1}$ (both calibrated with the Rayleigh line and the 521 $cm^{-1}$ line of a silicon standard). The Raman spectra were taken in confocal mode from $2 \times 2 \times 2$ μm sample volumes, using a Leica DMLM microscope and a Leica 50×/0.75 or 100×/0.90 objective. Instrument control and data acquisition were done with the Grams/32 software produced by Thermo Galactic Corporation (now Thermo Fisher Scientific).

## RESULTS

After providing supporting evidence for a lunar origin for the investigated meteorite, we then present its main petrographic characteristics.

### Lunar Origin

NWA 11962 was acquired by the NHM Vienna from a Moroccan meteorite dealer as a single stone, $5.5 \times 4.5 \times 2.0$ cm in size, with a total mass of 85 gram. The specimen (sample NHMV-N9595) does not show any obvious fusion crust, even though it contains features resembling regmaglypts and exhibits a black shiny surface with dull brownish areas (Figs. 1a and 1b). A cut and polished surface reveals that the interior of the meteorite consists of mainly submillimeter sized light-colored clasts and a black compact area of impact melt, suspended in a fine-grained, dark-gray matrix (Fig. 1a).

Oxygen isotope analysis was performed at the Open University Milton Keynes on two subsamples from NWA 11962 provided by the NHM Vienna. Lunar samples lie on or very close to the terrestrial fractionation line. Deviations from the terrestrial fractionation line can be expressed using the linearized formulation of $\Delta^{17}O$ (Miller 2002) where $\Delta^{17}O = 1000\ln(1 + [\delta^{17}O/1000]) - \lambda 1000\ln(1 + [\delta^{18}O/1000])$ where $\lambda = 0.5247$. The oxygen isotope composition (Fig. 2a) of NWA 11962 is consistent with a lunar origin ($\delta^{17}O = 3.14 \pm 0.04‰$, $\delta^{18}O = 6.03 \pm 0.05‰$, and $\Delta^{17}O = -0.02 \pm 0.01‰$ [all errors 1σ]).

The bulk FeO/MnO ratio calculated from EPMA data of the glassy matrix is 74.4, and, therefore, slightly higher than the mean FeO/MnO ratio of lunar meteorites (71.5) reported by Korotev (2005). Higher bulk FeO/MnO ratios have also been observed for other lunar meteorites; see, for example, Collareta et al. (2016). The arithmetic mean values of the atomic Fe/Mn ratios for pyroxene (59) and olivine (100) in NWA 11962 are in good agreement with the values for pyroxene (62) and olivine (103) from lunar basalts and clearly differ from values for pyroxene (Fe/Mn = 40) and olivine (Fe/Mn = 75) in terrestrial basalts (Papike et al. 2003). As shown in Figs. 2b and 2c, the Fe/Mn ratios of pyroxene and olivine grains in NWA 11962 clearly plot on the lunar trend line. In addition, the meteorite contains several lithologies that are typical of a lunar regolith breccia and are not known for terrestrial rocks in this particular form. These

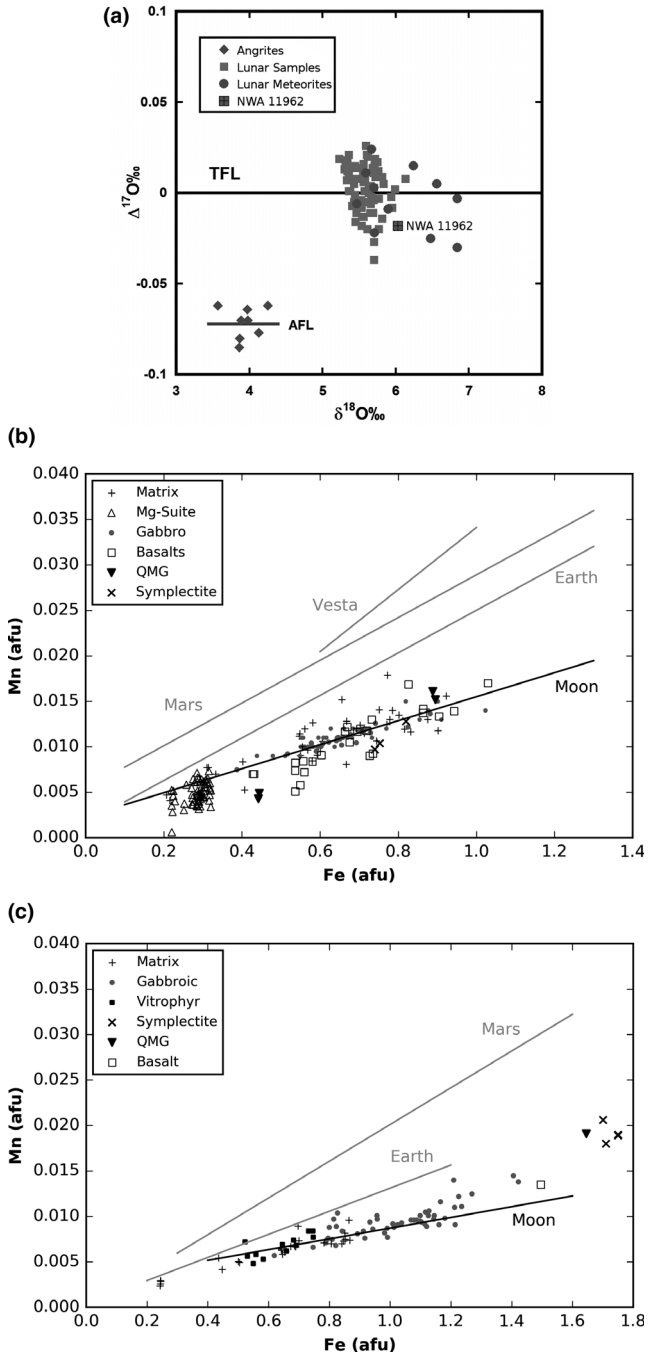


Fig. 2. Evidence for the lunar origin of NWA 11962. a) Oxygen isotopic composition of NWA 11962. The meteorite clearly plots in the field of lunar samples and other lunar meteorites at the terrestrial fractionation line (TFL). For comparison, the field of angrites is also shown (Greenwood et al. 2017). References for the data on lunar meteorites and lunar rocks are from the Meteoritical Bulletin. Fe and Mn ratios of (b) pyroxene and (c) olivine in monomineralic (matrix) and lithic clasts from NWA 11962 as obtained using the electron microprobe. Trend lines are taken from Karner et al. (2006; pyroxene) and Papike et al. (2009; olivine). QMG = quartz monzogabbro.

observations, and the petrological characteristics discussed in detail below, clearly confirm a lunar origin of NWA 11962.

## Petrographic Description

Thin sections NHMV-O266 and NHMV-O267 (see Figs. 1c–f) were cut from the same end of the meteorite specimen; thus, they represent serial sections. Both thin sections show a clast-rich (>25 vol%) breccia with fine-grained (0.03–0.3 mm) to medium-grained (0.3–3.0 mm) monomineralic and lithic clasts and, in the case of NHMV-O266, some glass fragments. The matrix consists of highly vesicular orange-brown glass (in plane-polarized light), which contains schlieren or appears as a coherent opaque (in transmitted light) area. Fragments of orange vitrophyric glass as well as orange and black glass spherules (as seen in plane-polarized light) are observable in thin section NHMV-O266. See Table S2 in supporting information for a petrographic overview of the different clasts as seen in the two thin sections investigated. No distinctive agglutinates were found. The lack of fusion crust is confirmed in thin section. All clasts display a certain degree of shock. Shock-induced modifications include fracturing, undulose extinction, and mosaicism of most silicate minerals. No planar fractures or planar deformation features were detected in the investigated minerals, but these shock-diagnostic features are relatively rare in lunar samples. Point counting (1000 points) of a BSE image from thin section NHMV-O266 (Fig. 1d) revealed an area distribution of 35% glassy matrix, 61% clasts, and 4% voids. NWA 11962 has to be classified as a lunar regolith breccia, because it contains several glass spherules. The large number of vesicles is also a distinctive feature of regolith breccias (Stöffler et al. 2006). Backscattered electron (BSE)-SEM images of both thin sections (Figs. 1d and 1f) reveal light gray areas contrasting with darker areas, reflecting the presence of gabbroic and more silica-rich domains, respectively. In some cases, minerals, or at least their rims, reacted (thermal digestion) with the impact melt that forms the matrix. Terrestrial weathering is indicated by the presence of calcium carbonate filling large cracks.

## Mineralogy

Individual mineral clasts embedded in the matrix of NWA 11962 include pyroxene, plagioclase, olivine, K-feldspar, silica (both quartz and tridymite as confirmed with micro-Raman; see Fig. 3), spinel, ilmenite, zircon, zirconolite, troilite, Fe-Ni metal, and barringerite.

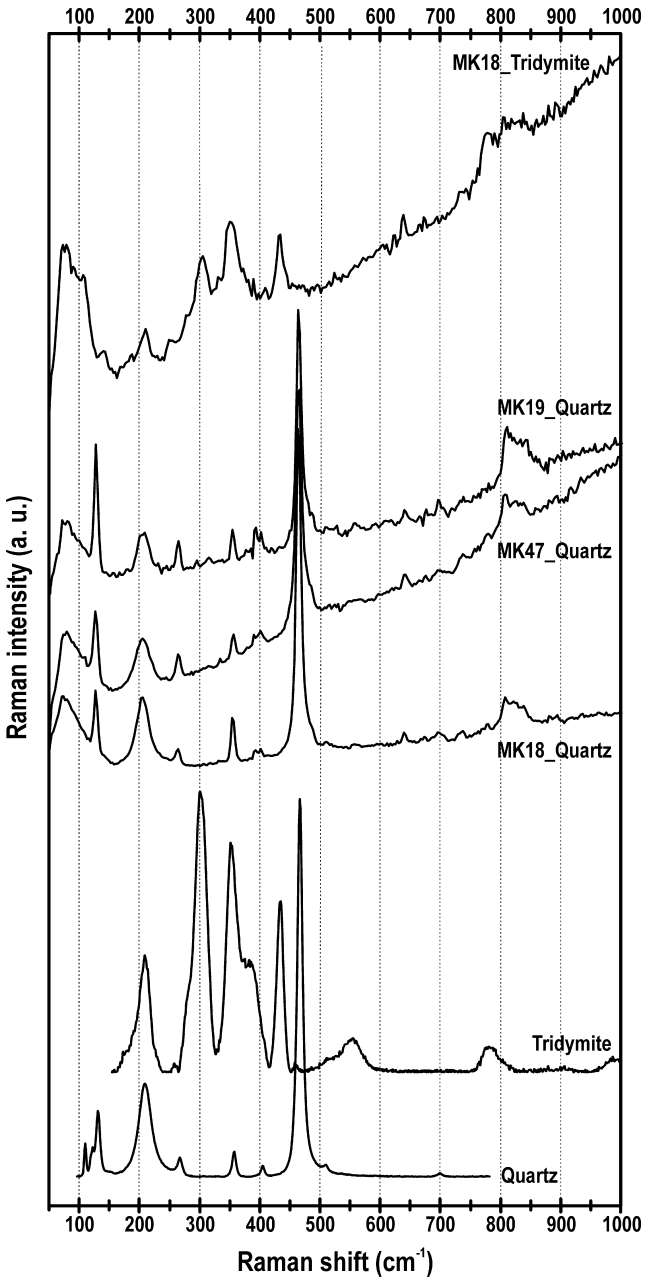


Fig. 3. Selected micro-Raman spectra of quartz and tridymite from some of the investigated clasts. Tridymite and quartz were noted in the case of the largest monomineralic silica (amorphous, quartz, and tridymite) clast (MK18) in the investigated thin sections. Only quartz was found in clast MK19 (i.e., a symplectite-like intergrowth of pyroxene, olivine, and quartz). Note that if this clast would have formed from the breakdown of pyroxferroite, tridymite would be expected to be present (see Lindsley et al. 1972). Quartz was also found in clast MK47, a small lithic clast (either a felsite or a quartz monzogabbro). Quartz (RRUFF ID_R040031) and tridymite (RRUFF ID_R090063) reference spectra from the RRUFF database (see Lafuente et al. 2015) are shown (at the bottom of the figure) for comparison.

### *Feldspar*

Plagioclase ($An_{53–98}Or_{0.0–2.5}$) is mostly anorthitic, especially in the basalts and the monomineralic clasts embedded in the glassy matrix. The gabbroic and quartz monzogabbro (QMG) clasts have a more sodium-rich composition (see Fig. 4a). K-feldspar was not found as isolated mineral fragments in the glassy matrix. All measured K-feldspar compositions shown in Fig. 4a are from lithic clasts (granophyric intergrowths with silica or basalt). These K-feldspars ($An_{3–6}Ab_{13–30}Or_{63–83}$) contain Ba ranging from 2.8 to 6.5 mol%, hereafter expressed as Celsian component (Cn).

### *Pyroxene*

Pyroxene is present both as monomineralic clasts or components of lithic clasts (see Fig. 4b), showing a wide range in compositions, and locally displaying exsolution lamellae. Pyroxene crystals in basalts show zoning, whereas pyroxene grains with exsolution lamellae are common in the QMG and the felsite clasts. The composition of pyroxenes in the basalts and as mineral clasts in the breccia range from pigeonite ($Fs_{28–41}Wo_{5–20}$, FeO/MnO = 44–76) to augite ($Fs_{11–47}Wo_{22–45}$, FeO/MnO = 41–96). As can be seen from Fig. 4b, there is a very striking cluster of pyroxenes with low-Ca and high-Mg contents ($Fs_{11–16}Wo_{0.9–3}$, FeO/MnO = 41–96). They solely occur as monomineralic clasts in the breccia and cannot be directly associated with any of the lithologies found in the breccia. Exsolved pyroxenes in the QMG and felsite clasts and exsolved pyroxene occurring as monomineralic clasts in the breccia have similar compositions ranging from $Fs_{56–70}Wo_{2–5}$ (FeO/MnO = 59–79) in the host to $Fs_{29–39}Wo_{35–44}$ (FeO/MnO = 55–113) in the augite exsolution lamellae, as typical of the so-called "inverted pigeonite." The $Al_2O_3$ concentration of the pyroxenes is mainly below 2 wt% and the $Cr_2O_3$ concentrations are mainly below 1 wt%.

### *Olivine*

Olivine is less abundant than pyroxene and plagioclase, but occurs throughout the breccia in both monomineralic and lithic clasts. The composition of olivine ranges between $Fa_{12}$ and $Fa_{87}$ (Fig. 4c) with FeO/MnO = 79–136.

### *Minor Phases*

Free silica is found in the granophyric intergrowths, in the QMG clast and QMG fragments, as monomineralic clasts in the breccia, and in symplectites. Some of the monomineralic silica clasts show numerous inclusions of presumably troilite. The spinel in the breccia has compositions ranging from chromite to ulvöspinel. Nearly endmember ulvöspinel is present, but rare. Spinel also occurs as an accessory phase in some

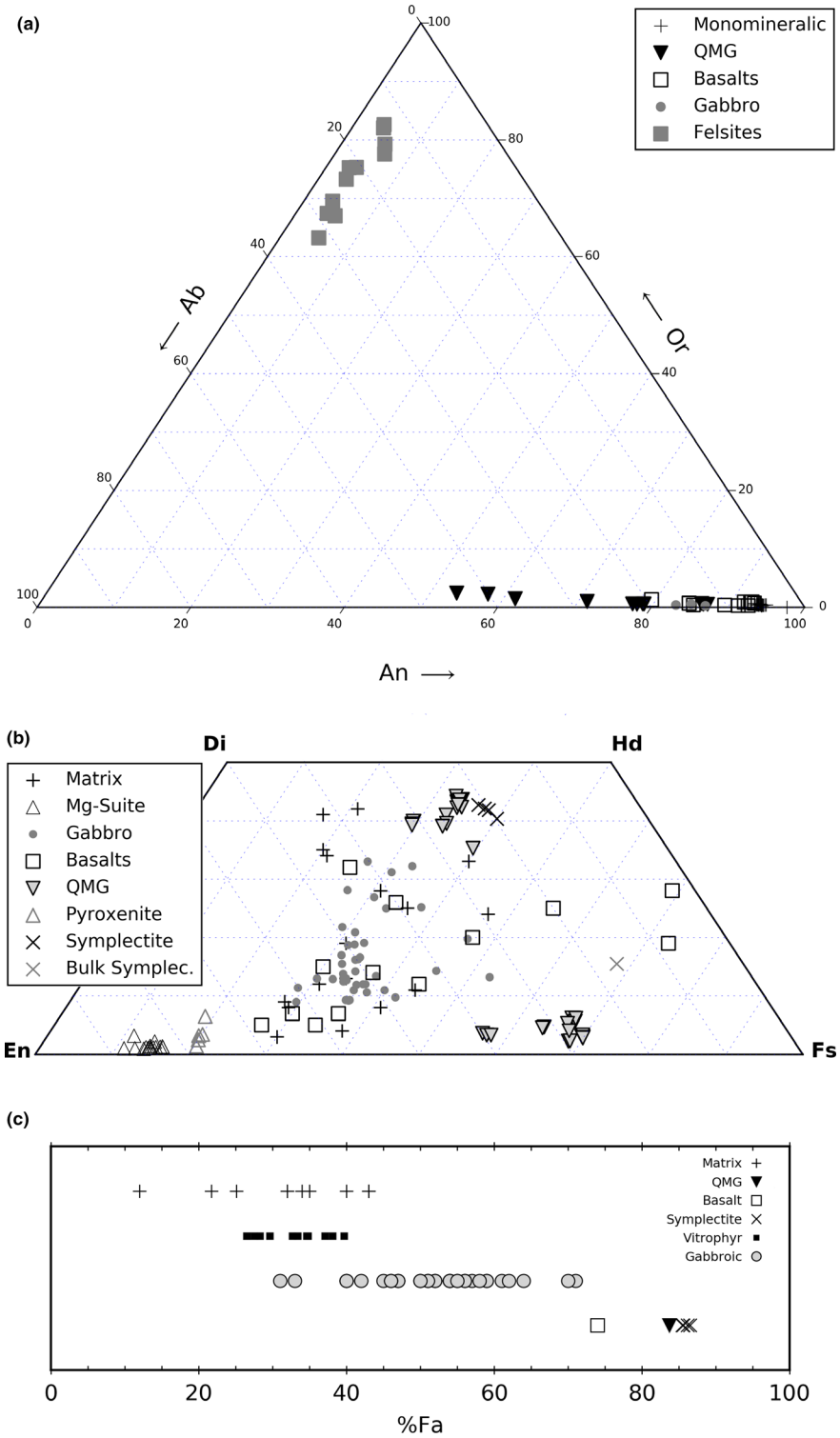


Fig. 4. Mineral chemistry of clasts in NWA 11962. a) Ternary feldspar diagram showing the compositions of K-feldspar and plagioclase from monomineralic and lithic clasts of NWA 11962. b) Quadrilateral plot of pyroxene compositions from monomineralic and lithic clasts as found in NWA 11962. c) Fayalite content in olivine in clasts from NWA 11962. All data obtained by electron microprobe. Plots (a) and (b) were partially made using the Python package "python-ternary" (Harper 2020).

basalt and gabbroic clasts. Ilmenite is the most abundant opaque phase in both thin sections. Some of the ilmenite is magnesium-rich, containing up to ~8 wt% MgO. Another relatively abundant accessory mineral is zircon, with grain sizes mostly in the range from 10 to 30 μm. Thin section NHMV-O267 contains one large zircon crystal that is approximately 50 × 140 μm in size. Rare zirconolite is also present in both thin sections. Furthermore, the investigated thin sections contain troilite and Fe-Ni metal, mostly as kamacite. Additionally, there is at least one large (approximately 100 × 60 μm) grain of nickel-free native iron. The calcium phosphate mineral whitlockite appears as inclusions in some high Mg# pyroxenes. The thin section NHMV-O266 contains one small grain (approximately 38 × 28 μm) of barringerite ($Fe_{1.96}Ni_{0.2}S_{0.2}$)P, a very rare iron phosphide mineral, whose occurrence in lunar rocks was first reported by Brandstätter et al. (1991).

### Gabbroic Clasts

The most conspicuous and largest constituents in the breccia are gabbroic clasts. In BSE maps of the thin sections (Figs. 1d and 1f), these clasts are recognizable by their comparatively coarse grain size and bright appearance. Locally, gabbroic clasts appear partially molten and are opaque in transmitted light (Figs. 1c and 1e). More than half of the surface area of thin section NHMV-O267 is occupied by these gabbroic clasts (middle part of Fig. 1d). As can be seen in detail from Figs. 5a and 5b, these clasts have a medium-grained, equigranular texture, composed of pyroxene, plagioclase, and olivine, with crystal sizes up to 1 mm in the longest dimension. Accessory phases include large ilmenite grains and some spinel crystals. Pyroxene ($En_{34–62}Fs_{20–46}Wo_{9–35}$) and olivine ($Fa_{29–73}$) crystals are strongly zoned. Plagioclase ($An_{84–88}Ab_{12–16}Or_{0.3–0.8}$) has a relatively homogenous composition. The chemical zoning of the mafic phases is altered by glassy shock veins pervading the crystals. Some of these clasts may belong to the same larger clast in 3-D, considering their extension in the thin sections and their similar chemical composition.

### Basalt Clasts

A few basaltic clasts, mainly of small size (up to approximately 0.5 mm) and different compositions, occur throughout the breccia. For an overview of their mineral chemistry, see Table 1. The identification of these clasts as magmatic rocks is based on their texture. However, we cannot exclude that some of these clasts could be fragments of impact melt rocks that underwent recrystallization. Two representative clasts of this sort are described here in detail. Clast LK2 (Fig. 5c) is 550 × 425 μm in size and shows subophitic texture with plagioclase laths encompassing pyroxene crystals. Accessory phases include K-feldspar, ilmenite, spinel, and troilite. The zoned pyroxenes have a more magnesium-rich core ($En_{41–56}Fs_{30–38}Wo_{12–26}$) and an iron-rich rim ($En_{41–44}Fs_{42–45}Wo_{12–17}$). Plagioclase crystals are anorthitic ($An_{92–96}$). The bulk Mg# for the LK2 clast is 51, similar to Apollo 14 high-Al and very high-K basalts (Neal and Taylor 1992). With an $Al_2O_3$ content of 15 wt%, a $TiO_2$ content of 2 wt%, and a $K_2O$ content of 6400 ppm, this basalt clast can be classified as an aluminous, low-Ti, and high-K basalt (Warren and Taylor 2014) or very high-K basalt ($K_2O$ >0.5 wt%), respectively. Basalt clast LK3 has an annealed texture, with grain boundaries having 120° angles that indicate that it has (re)crystallized. The size of the clast is approximately 460 × 410 μm. It is composed of plagioclase, pyroxene, and ilmenite with angles between mineral grains often near 120°. The pyroxene crystals do not show a strong zoning from core ($En_{57}Fs_{36}Wo_7$) to rim ($En_{60}Fs_{35}Wo_5$) and the anorthite content of plagioclase ranges from $An_{85}$ to $An_{89}$.

### Recrystallized Impact Melt Globule

Thin section NHMV-O266 contains one ovoid-shaped globule (LK1) with a size of 900 × 750 μm without any indication of broken surfaces. It has an intersertal texture (Fig. S1 in supporting information), formed by plagioclase laths accompanied by pyroxene, olivine, and ilmenite in the interstices. Plagioclase compositions vary between $An_{79}$ and $An_{85}$. Pyroxene crystals are zoned and vary greatly from core ($En_{43–58}Fs_{22–37}Wo_{6–34}$) to rim ($En_{3–43}Fs_{25–73}Wo_{16–32}$), whereas olivine grains are iron-rich ($Fa_{74}$).

### Quartz Monzogabbro (QMG)

Thin section NHMV-O266 contains a unique QMG clast (LK10) approximately 650 × 500 μm in size (Fig. 5d). In earlier literature, lunar QMG was somewhat misleadingly referred to as quartz monzodiorite (QMD) even if the anorthite content of the involved plagioclase was higher than 50% (Papike et al. 1998). The texture of the clast seems poikilitic (in BSE images), with plagioclase ($An_{52–84}Ab_{16–46}Or_{0.4–2.2}$) enclosing pyroxene, K-feldspar ($An_{1–10}Ab_{13–21}Or_{73–85}Cn_{2–4}$), silica, minor olivine ($Fa_{84}$), and accessory phases such as zircon, ilmenite, and troilite. The exsolved pyroxenes consist of 5 μm thick augite ($En_{23–24}Fs_{36}Wo_{39–40}$) lamellae in an iron-rich low Ca-pyroxene ($En_{26}Fs_{69–70}Wo_4$) host with Fe# ranging from 60 to 72 (inverted pigeonite). Point

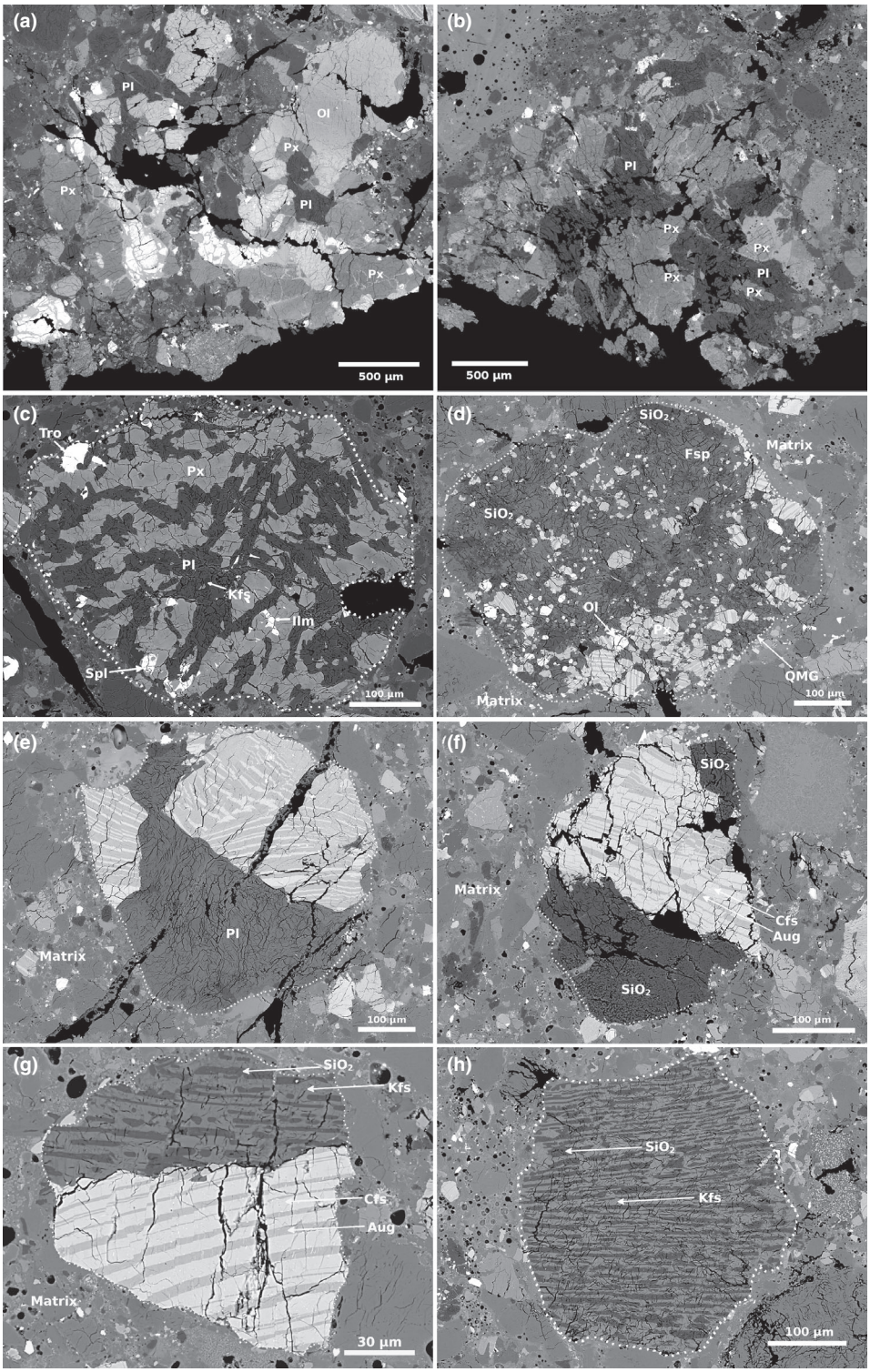


Fig. 5. Backscattered electron images of clasts in NWA 11962. a, b) Gabbroic clasts in thin sections NHMV-O266 and NHMV-O267. c) Aluminous, low-Ti, very high-K, basalt clast with subophitic texture. d) Quartz monzogabbro (QMG) clast. e) QMG fragment. f, g) QMG or felsite fragments. h) Felsite clast (granophyric intergrowth of silica and K-feldspar). Aug = augite; Cfs = clinoferrosilite; Fsp = feldspar; Ilm = ilmenite; Kfs = K-feldspar; Ol = olivine; Pl = plagioclase; Px = pyroxene; Spl = spinel; Tro = troilite. The black areas on the images are either vesicles or areas where material was lost during thin section preparation.

Table 1. Feldspar, pyroxene, and olivine compositions of different lithic clasts from NWA 11962. $K_2O$ abundances and Mg# data are approximated bulk clast values from EDS analyses, except for basalt LK2, where they are calculated values, based on the abundance of K-feldspar as evaluated from image analysis.

| Classification | Clast | Texture | An | Or | An average | En | Fs | Wo | Cpx Mg# | Opx Mg# | Fo | Fo average | $K_2O$ wt% | Mg# |
|---|---|---|---|---|---|---|---|---|---|---|---|---|---|---|
| Gabbro | LK20 | Equigranular | 83–87 | 0.3–0.6 | 85.3 | 38–62 | 27–45 | 9–33 | 47–68 | – | 47–59 | 52.3 | – | – |
| Basalt | LK2 | Subophitic | 92–93 | 0.6–0.9 | 92.4 | 41–56 | 30–38 | 12–26 | 47–64 | – | – | – | 0.6 | – |
| Basalt | LK1 | Intersertal | 79–85 | 0.4–1.7 | 81.7 | 20–44 | 22–55 | 25–34 | 26–66 | – | 26 | – | 0.6 | 22 |
| Basalt | LK3 | Subophitic | 85–89 | 0.4–0.7 | 86.5 | 57–60 | 34–36 | 5–7 | – | 61–64 | – | – | 0.5 | 46 |
| Basalt | S12 | Subophitic | 91–92 | 0.9–1.5 | 92.0 | 33–49 | 37–47 | 14–20 | 41–57 | – | – | – | 0.5 | 38 |
| Basalt | LK4 | Subophitic | 90–93 | 0.3–0.4 | 91.3 | 68–69 | 27 | 4–5 | – | 71–72 | – | – | – | – |
| QMG | LK10 | Poikilitic? | 5–78 | 0.6–81 | 51.8 | 23–27 | 36–70 | 4–40 | 39–40 | 27–28 | 16 | – | 2.1 | – |
| QMG | MK3 | Fragment | 58–80 | 0.6–2.4 | 62.1 | 22–27 | 34–70 | 3–43 | 39–40 | 27–28 | – | – | – | – |
| QMG | MK28 | Fragment | 37–67 | 22–45 | 54.3 | 24–28 | 34–67 | 5–42 | 41 | 29 | – | – | – | – |
| QMG | MK56 | Fragment | 74–75 | 0.7–0.9 | 74.6 | 27–31 | 35–64 | 5–39 | 54 | 33 | – | – | – | – |
| QMG | MK60 | Fragment | 2.2–23 | 71–89 | 11.9 | 24–27 | 33–69 | 5–43 | 42 | 28 | – | – | – | – |
| Felsite | MK8 | Granophyric | 3–4 | 67–75 | 3.5 | – | – | – | – | – | – | – | – | – |
| Felsite | MK40 | Granophyric | 3–6 | 73–84 | 5.6 | – | – | – | – | – | – | – | – | – |

counting resulted in a modal composition of 58% feldspar, 21% pyroxene, 19% silica, and 2% accessory phases. Thin section NHMV-O266 also contains several clasts which are obviously QMG fragments (see, e.g., Figs. 5e–g). These QMG fragments appear to have larger grain sizes than the large QMG clast (LK10) discussed above.

### Felsite (Lunar Granite)

Both thin sections contain felsite clasts, which are also referred to as lunar granite. Lunar granites differ from terrestrial granites in both texture and mineralogy. However, the term is used for lunar rocks and fragments that have similar silica contents ($SiO_2$ >65 wt%) as terrestrial granites (Ryder et al. 1975). Thin section NHMV-O267 only contains a few small felsite clasts up to 200 μm in size. Thin section NHMV-O266 on the other hand has abundant felsite clasts with sizes from 400 μm down to 20 μm or even smaller but then optically not recognizable as granites anymore. One of the largest clasts is shown in Fig. 5h. Its texture can be described as a granophyric intergrowth of silica and K-feldspar, where the silica forms a "ribbon-like" almost parallel structure to the K-feldspar. The composition of the K-feldspar ($An_{3–8}Or_{67–78}Ab_{12–26}Cn_{2–6}$) varies slightly from one clast to another. The silica phase in lunar felsites is usually quartz but cristobalite has also been reported (see e.g., Robinson and Taylor 2011; Seddio et al. 2015). Unfortunately, we were not able to obtain any suitable micro-Raman data for this type of clasts (i.e., due to previous SEM and microprobe imaging and mapping of these clasts), and, thus, we cannot confirm whether it is quartz and/or cristobalite. Some of the clasts have rod-shaped, opaque inclusions, which for their size (2–3 μm in diameter) could not be accurately analyzed. However, semiquantitative analyses of their chemical composition, although contaminated by the host mineral, suggest the presence of zirconolite.

### High Mg# Pyroxenes

Thin section NHMV-O266 contains abundant monomineralic clasts of pyroxene with high Mg# (85.5 ± 1.3). The chemical composition of these clasts is shown in Figs. 2b, 4b, and 6b. There is no evidence that these pyroxenes are associated with other rock-forming minerals composing a known Mg-suite lithology. The high Mg# pyroxenes show small exsolution features, as can be seen in Fig. S2 in supporting information, and mineral inclusions, such as chromite (white blebs in Fig. S2a) and whitlockite (Fig. S2b).

### Pyroxenite

Thin section NHMV-O266 contains one large (1.1 × 0.6 mm) pyroxenite clast. It consists of low-Ca pyroxene crystals with compositions $En_{75–78}Fs_{19–20}Wo_{1–6}$. The individual crystals are oriented randomly and contain thin lamellae, not more than a few hundred nanometers thick, which appear opaque in plane-polarized light (see Fig. S3 in supporting information). Some of the pyroxene grains contain small accessory minerals, consisting of ilmenite, chromite, feldspar, and possibly armalcolite.

### Symplectite

Thin section NHMV-O266 contains at least two clasts with a symplectitic appearance. One is approximately 350 μm (Fig. 7) and the other one only

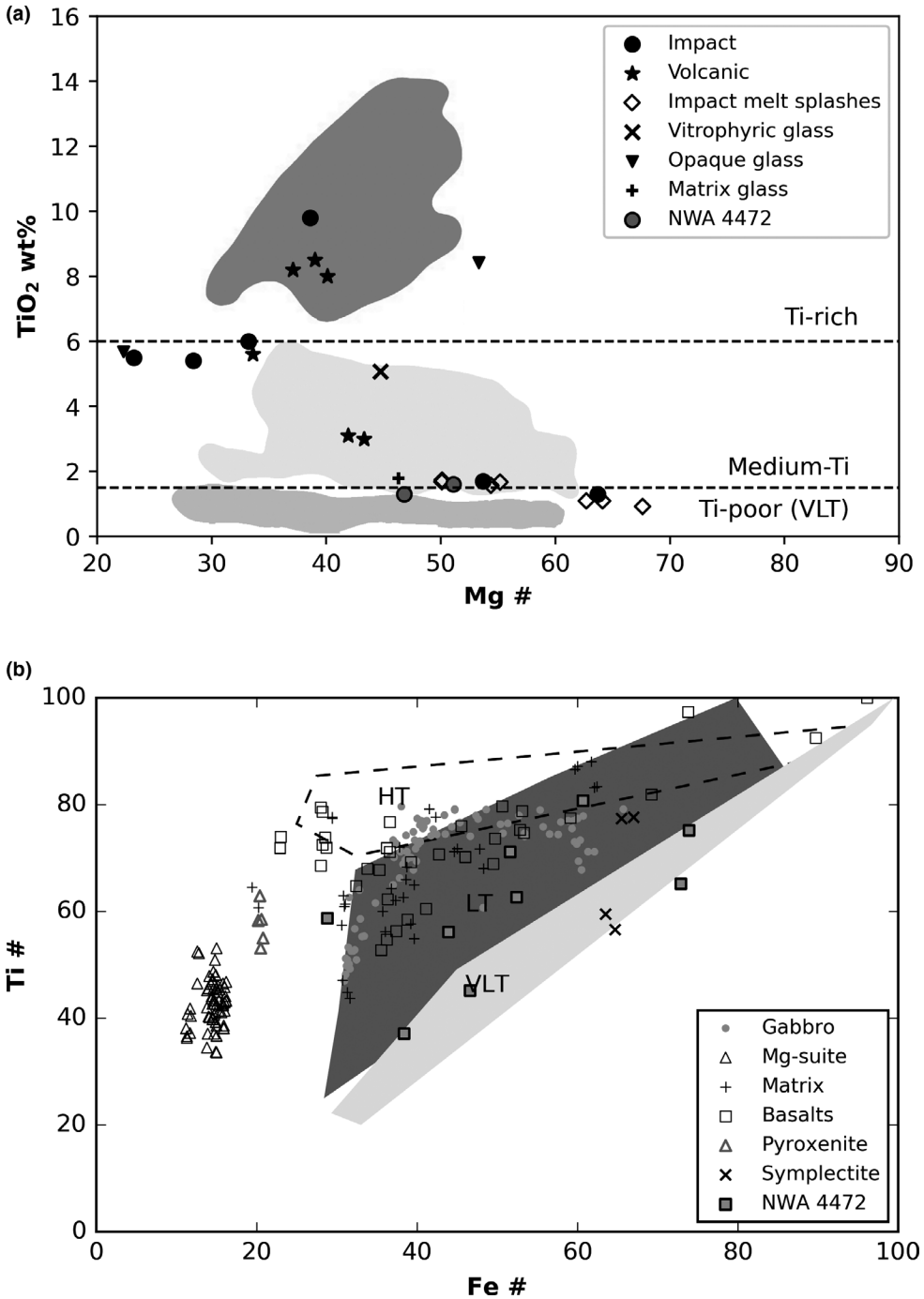


Fig. 6. Comparison of clasts in NWA 11962 with different lunar basalt suites. a) Plot of Mg# versus $TiO_2$ showing fields for mare basalts and picritic glasses as in Neal and Taylor (1992). Filled circles and stars represent impact-related and volcanic glass beads, respectively. For comparison, the two (impact) glass beads values reported from NWA 4472 (Joy et al. 2011) are shown. b) Ti# (Ti/Ti + Cr) versus Fe# (Fe/Fe + Mg) plot for pyroxenes in clasts from NWA 11962 and NWA 4472 (filled squares) compared with fields for lunar basalt (Nielsen and Drake 1978). Compositional fields for the basalts are from Papike et al. (1991).

70 μm in size. In both cases, the symplectite-like clasts consist of an intergrowth of hedenbergitic pyroxene ($En_{20–21}Fs_{36–40}Wo_{40–43}$), Fe-rich olivine ($Fa_{86}$), and quartz (as confirmed with micro-Raman; see Fig. 3). A modal analysis of the clasts in NWA 11962 revealed a bulk composition of approximately $(Fe_{0.55}Ca_{0.13}Mg_{0.13}Mn_{0.01})SiO_3$ corresponding to an equivalent pyroxene composition $En_{16.5}Fs_{68}Wo_{15.5}$.

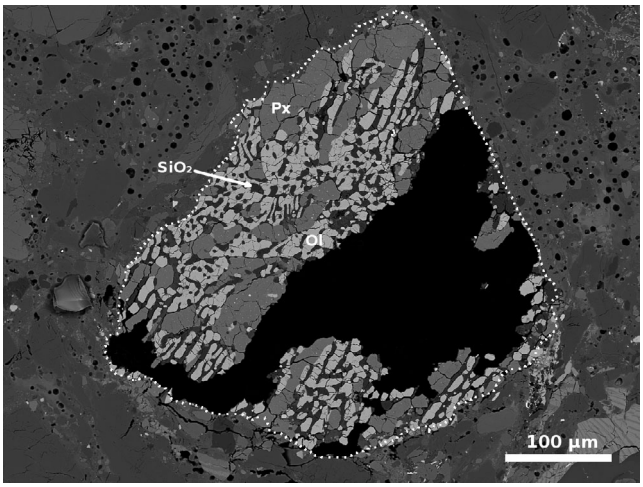


Fig. 7. BSE image of a symplectite clast in the matrix of NWA 11962 comprising pyroxene (gray), olivine (light gray), and silica (dark gray). Micro-Raman spectroscopy confirms that the $SiO_2$ in this clast is quartz. Ol = olivine; Px = pyroxene. Abundant vesicles can be seen as black dots in the matrix surrounding the clast. The large black area corresponds to material that was removed during thin section preparation.

## Glass Spherules

Thin section NHMV-O266 contains at least 12 glass spherules, which led to the classification of NWA 11962 as a regolith breccia (Meteoritical Bulletin, No. 107). Some spherules have a homogeneous appearance without schlieren or inclusions, whereas others are partially or completely recrystallized, showing submicrometer dendritic crystals and/or inclusions (Figs. 8a, 8b, and S4 in supporting information). However, all spherules contain one or several vesicles, indicating an excess gas phase (Rutherford et al. 2017). The largest spherule found has a diameter of approximately 130 µm. The chemical composition of these spherules is provided in Table 2. Their chemical composition is internally quite homogeneous, but shows significant differences between spherules. On a compositional basis, the glass spherules can be divided into at least three distinct groups for the impact glass spherules and also three distinct groups for the volcanic spherules. Volcanic and impact-related spherules can be distinguished using the Mg/Al ratio; If Mg/Al is >1.5, the spherules can be assumed to be volcanic in origin, otherwise they are considered as impact-related (see, e.g., Delano and Livi 1981; Delano 1986). Six of the investigated spherules listed in Table 2 can be classified as volcanic. These volcanic spherules also have higher Mg/Ca ratios, as well as higher Fe and Cr concentrations than the impact spherules (Table 2). As can be seen from Fig. 6a, all spherules but one (SP6) has intermediate (1.5–6 wt%) to high $TiO_2$ (>6 wt%) concentrations. In plane-polarized light, none of the volcanic spherules are orange, but rather blackish in color. The impact spherules are yellow/orange (see Fig. 8a) and black in color. Mg# values range from 33 to 64 in the impact spherules and from 34 to 43 in the volcanic spherules (Table 2), respectively. Spherule SP6 is an exception in that it is colorless and has the highest Mg# value (64), aside from having the lowermost $TiO_2$ content (1.3 wt%) among the investigated spherules.

## Olivine Vitrophyric Glasses

Thin section NHMV-O266 contains a few olivine vitrophyre clasts. The largest of these olivine vitrophyres has a size of 0.7 × 1.5 mm. They consist of 20–50 µm sized olivine crystals with a skeletal appearance and tiny opaque minerals, most likely Cr-rich spinel crystals (1–5 µm), with a euhedral (rhomboidal) shape, embedded in a yellowish to brownish (in plane-polarized light) glass matrix (Figs. 8c and 8d). The crystals have a random distribution and do not show any flow fabric. The vitrophyric glass is surrounded by a dark and opaque rim, which recalls chilled margins. As can be seen using the BSE mode (see Fig. 8d), all olivine crystals are permeated by numerous fractures, which do not propagate into the glass matrix.

## Impact Melt Splashes

In addition to the glass spherules discussed above, NWA 11962 contains several glassy impact melt splashes with an amoeboid shape (Figs. 8e and S5 in supporting information). They contain only a few mineral clasts incorporated at the rims. The glass has no schlieren and does not show hints of recrystallization. Unlike the impact spherules, the impact melt splashes have a very homogenous chemical composition (see Table 3). The Mg/Al ratios are well below 1.5, supporting their impact origin. In addition, all impact melt splashes have low $TiO_2$ values comparable to the $TiO_2$ concentration in the bulk meteorite. In general, their chemical composition is very similar to the bulk chemistry of the meteorite as measured in the impact melt matrix (see Table 3).

## Impact Breccias and Granulites

NWA 11962 contains few impact breccia and granulite clasts, mostly of small size. Examples are shown in Figs. S6 and S7 in supporting information. Some petrographic details are given in Table S2.

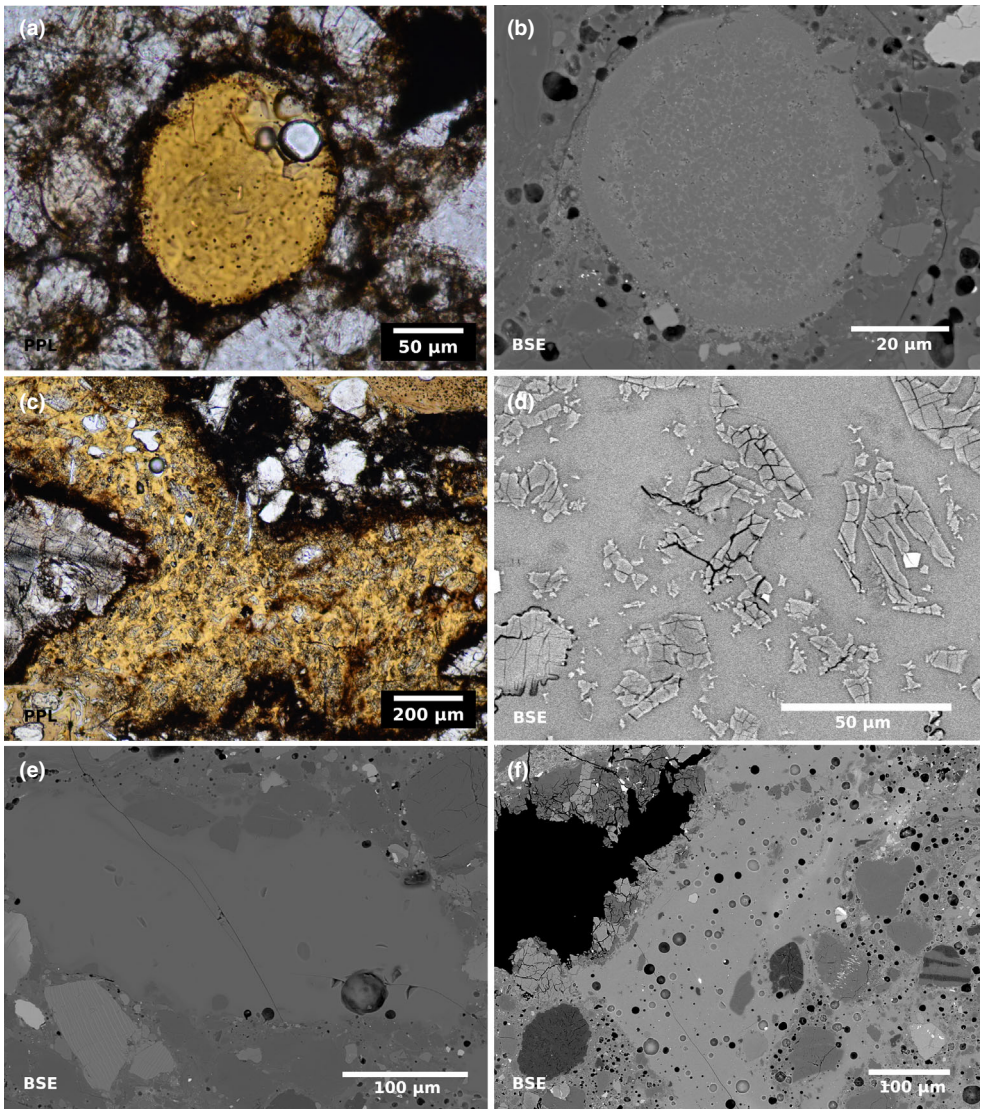


Fig. 8. Different types of glass found in NWA 11962. a) Impact melt spherule in plane-polarized light (PPL) as seen under the optical microscope. b) Backscattered electron (BSE) image of a volcanic spherule. c) Olivine vitrophyric glass in PPL under the optical microscope. d) BSE image showing details of the olivine vitrophyric glass. e) BSE image of an impact melt splash. f) BSE image of an impact melt vein and the glassy impact melt matrix, both with abundant vesicles. Note also the silica (dark gray) and felsite clasts typical for NWA 11962.

## DISCUSSION

### Potpourri of Clasts and Their Source Regions

#### *Gabbroic Clasts*

These clasts clearly have been altered by impact melting, as suggested by the presence of multiple glassy shock veins crosscutting them. The mafic phases are not well equilibrated, such that their chemical composition differs throughout the sample. The observed chemical zoning of the mafic phases is primary and indicates crystallization at nonequilibrium conditions. Therefore, these clasts could be of hypabyssal origin or are derived from a shallow intrusion. An origin from a very thick lava flow was also considered for similar lunar material by Day and Taylor (2007). Figure 6b shows that the pyroxenes in the gabbroic clasts correlate with low-Ti to high-Ti source magmas (Nielsen and Drake 1978). Interestingly, this corresponds well with the Ti concentrations in the volcanic glass beads (Fig. 6a). Taking into account that the gabbroic clasts are a major component in the thin sections of the regolith breccia investigated here, these observations point toward a low-Ti to high-Ti source region.

Table 2. Electron microprobe data for glass spherules in NWA 11962. Spherules with Mg/Al > 1.5 are considered to be of volcanic origin, whereas spherules with Mg/Al < 1.5 are considered to be of impact origin (see text). Oxide abundances in wt%.

| | Sp1 Orange Impact | Sp2 Black Volcanic | Sp3 Orange Impact | Sp4 Black Volcanic | Sp4a – Impact | Sp5 Black Impact | Sp6 Colorless Impact | Sp7 Black Volcanic | Sp8 Black Impact | Sp9 Black Volcanic | Sp10 – Volcanic | Sp0 – Volcanic |
|---|---|---|---|---|---|---|---|---|---|---|---|---|
| $SiO_2$ | 41.33 | 38.51 | 43.74 | 39.18 | 50.21 | 45.37 | 43.17 | 38.26 | 41.27 | 37.81 | 42.34 | 42.19 |
| $TiO_2$ | 5.98 | 8.00 | 5.43 | 5.58 | 1.69 | 5.54 | 1.28 | 8.51 | 9.84 | 8.16 | 3.03 | 3.12 |
| $Al_2O_3$ | 10.28 | 5.17 | 9.87 | 5.79 | 15.80 | 10.51 | 19.69 | 4.90 | 10.07 | 4.92 | 6.45 | 6.25 |
| $Cr_2O_3$ | 0.33 | 0.63 | 0.26 | 0.46 | 0.21 | 0.28 | 0.15 | 0.64 | 0.41 | 0.59 | 0.55 | 0.53 |
| FeO | 19.12 | 23.85 | 19.92 | 26.62 | 9.51 | 20.22 | 8.37 | 24.63 | 16.40 | 25.21 | 22.35 | 22.82 |
| MnO | 0.23 | 0.29 | 0.24 | 0.30 | 0.11 | 0.27 | 0.13 | 0.30 | 0.25 | 0.31 | 0.30 | 0.29 |
| MgO | 9.49 | 15.97 | 7.89 | 13.46 | 11.03 | 6.09 | 14.71 | 15.72 | 10.31 | 14.86 | 17.09 | 16.46 |
| CaO | 11.00 | 6.98 | 9.91 | 7.91 | 9.73 | 10.38 | 11.86 | 6.99 | 10.71 | 7.29 | 7.58 | 7.74 |
| $Na_2O$ | 0.16 | 0.27 | 0.78 | 0.19 | 0.52 | 0.56 | 0.03 | 0.23 | 0.40 | 0.20 | 0.15 | 0.28 |
| $K_2O$ | 0.03 | 0.04 | 0.19 | 0.09 | 0.35 | 0.34 | 0.01 | 0.03 | 0.02 | 0.08 | 0.04 | 0.02 |
| $P_2O_5$ | 0.08 | 0.07 | 0.16 | 0.11 | 0.04 | 0.32 | 0.09 | 0.06 | 0.06 | 0.08 | 0.05 | 0.06 |
| Total | 98.04 | 99.77 | 98.40 | 99.66 | 99.19 | 99.89 | 99.48 | 100.28 | 99.74 | 99.52 | 99.91 | 99.75 |
| Mg/Al | 1.2 | 3.9 | 1.0 | 2.9 | 0.9 | 0.7 | 0.9 | 4.1 | 1.3 | 3.8 | 3.4 | 3.3 |
| Mg/Ca | 1.2 | 3.2 | 1.1 | 2.4 | 1.6 | 0.8 | 1.7 | 3.1 | 1.3 | 2.8 | 3.1 | 3.0 |

Table 3. Chemical composition of impact melt splashes (IMS) and of the glass matrix in NWA 11962 as measured by EPMA. Oxide abundances in wt%.

| | IMS 1 | IMS 2 | IMS 3 | IMS 4 | IMS 5 | IMS 6 | IMS 7 | Matrix |
|---|---|---|---|---|---|---|---|---|
| $SiO_2$ | 49.28 | 47.58 | 49.58 | 50.84 | 50.16 | 50.91 | 44.11 | 46.78 |
| CaO | 9.96 | 10.26 | 9.89 | 10.05 | 9.38 | 10.06 | 11.97 | 11.60 |
| FeO | 7.04 | 7.33 | 9.36 | 9.19 | 9.27 | 9.03 | 7.95 | 9.79 |
| MnO | 0.10 | 0.12 | 0.12 | 0.13 | 0.10 | 0.11 | 0.15 | 0.13 |
| MgO | 12.59 | 15.31 | 11.52 | 9.24 | 11.05 | 9.06 | 13.37 | 8.44 |
| $Al_2O_3$ | 18.58 | 17.72 | 16.16 | 16.36 | 15.58 | 16.43 | 20.56 | 18.37 |
| $Cr_2O_3$ | 0.24 | 0.19 | 0.19 | 0.11 | 0.23 | 0.17 | 0.15 | 0.26 |
| $TiO_2$ | 1.09 | 0.92 | 1.67 | 1.73 | 1.57 | 1.68 | 1.09 | 1.79 |
| $Na_2O$ | 0.39 | 0.17 | 0.30 | 0.49 | 0.73 | 0.51 | 0.04 | 0.62 |
| $K_2O$ | 0.24 | 0.09 | 0.21 | 0.42 | 0.59 | 0.43 | 0.02 | 0.40 |
| $P_2O_5$ | 0.14 | 0.15 | 0.07 | 0.17 | 0.40 | 0.15 | 0.09 | 0.43 |
| Total | 99.67 | 99.85 | 99.12 | 98.74 | 99.08 | 98.60 | 99.54 | 98.63 |
| Mg/Al | 0.7 | 0.9 | 0.7 | 0.6 | 0.7 | 0.6 | 0.7 | 0.5 |
| Mg/Ca | 1.3 | 1.5 | 1.2 | 0.9 | 1.2 | 0.9 | 1.1 | 0.7 |

### *Basalt Clasts*

Pyroxenes in the basalt clasts are also of a low-Ti to high-Ti origin (see Fig. 6b). Basalt clast LK2 is from an aluminous, low-Ti and high-K basalt or very high-K basalt ($K_2O$ >0.5 wt%), respectively. Very high-K basalts (VHK) are known from Apollo 14 breccias (Shervais et al. 1983, 1984, 1985). We infer that these basalts were derived from low-Ti basalt magmas that assimilated components of granitic crust as they ascended to the lunar surface (Shervais et al. 1985). Based on a comparison of REE patterns of VHK and lunar granite samples, Neal et al. (1989) argued in the same direction for the origin of these basalts. This is interesting because NWA 11962 contains both this type of basalt clasts as well as lunar granites. Thus, from this point of view, they might also be spatially related, concerning their origin. This is worth mentioning, as it is not uncommon for regolith breccias, like NWA 11962, to contain components that originated from different locations and were merged by impact processes (e.g., McKay et al. 1991).

### *Recrystallized Impact Melt Globule*

Globules with a similar texture were reported for the granulitic breccia Dhofar 026 by Cohen et al. (2004) and

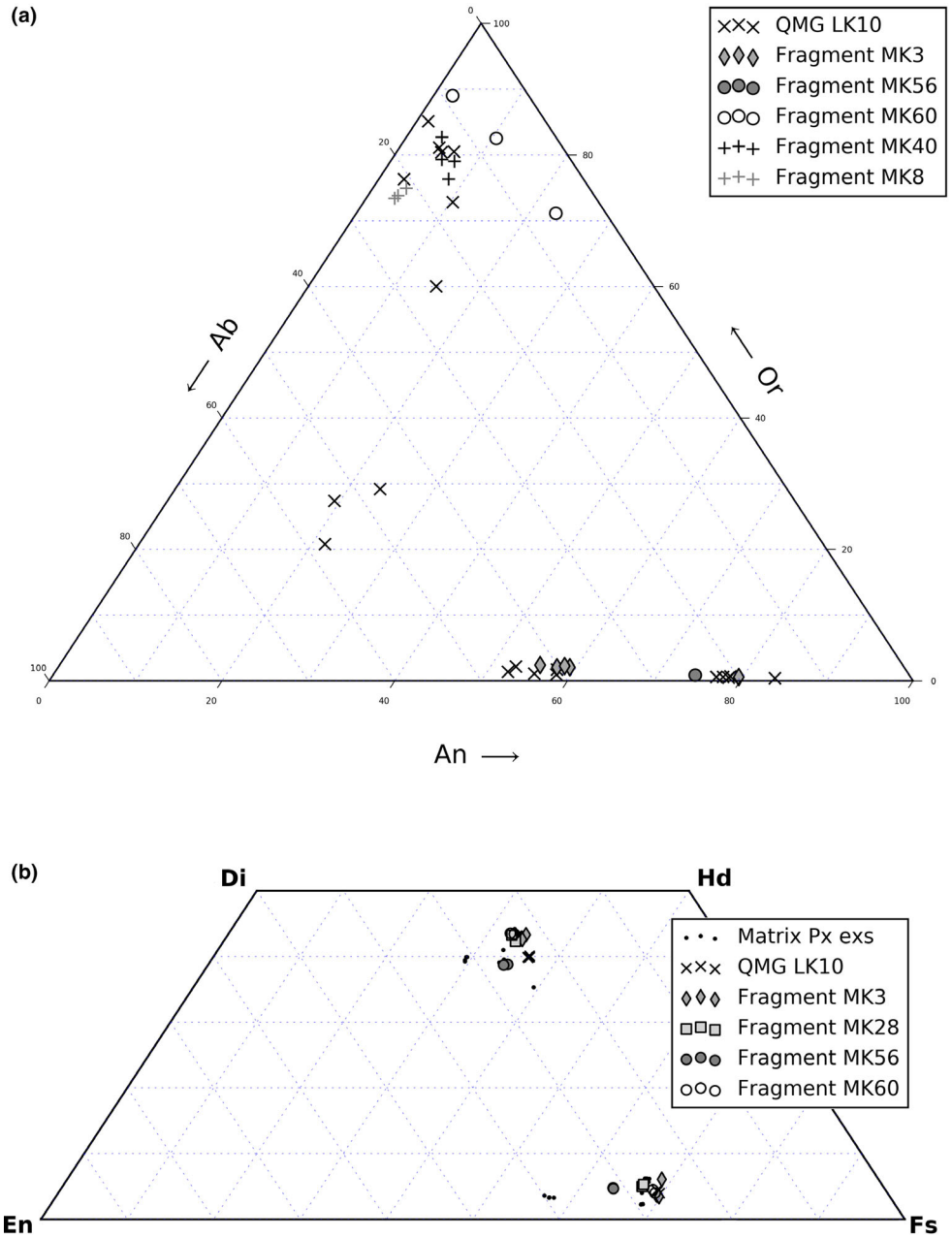


Fig. 9. Mineral chemistry of the large quartz monzogabbro (QMG) clast (LK10) and some smaller QMG and felsite fragments in thin section NHMV-O266 of NWA 11962. a) Feldspar composition and (b) pyroxene composition. All data obtained by electron microprobe. Matrix Px exs: Monomineralic exsolved pyroxene clasts in the breccia. Plots (a) and (b) were partially made using the Python package "python-ternary" (Harper 2020).

Warren et al. (2005). Cohen et al. (2004) concluded that these are recrystallized impact melt globules. Beside the similar texture, the mineral chemistry reported by these authors is quite different to the globule discussed here. The plagioclase in the globule in NWA 11962 is much more sodic ($An_{79}$–$An_{85}$) than the plagioclase in Dhofar 026 ($An_{92}$–$An_{95}$) globules. Furthermore, the olivine and pyroxene in the globule in NWA 11962 are much more iron-rich than in the globules in Dhofar 026. This difference in mineral chemistry points toward different source regoliths from which the globules formed.

### *Quartz Monzogabbro and Felsite Clasts*

The abundant QMG and felsite clasts are a very peculiar feature of the investigated regolith breccia. In general, they are rare lunar lithologies and it is still

unclear whether they formed as separate intrusive bodies or represent fragments from trapped melt-rich regions of other lunar rock types (Wieczorek et al. 2006). However, such types of clasts have never been found (as far as we are aware) in intergrowth with other rock types, such as basalts. The Fe# value is slightly higher than that reported for the pyroxenes from the QMG/QMD clasts of Apollo 15 (Fagan et al. 2014). The anorthite content of plagioclase ($An_{52}$–$An_{84}$) is comparable to other QMG/QMD clasts in the literature (e.g., Jolliff et al. 1999; Fagan et al. 2014; Hidaka et al. 2014). Several of the lithic clasts that are embedded in the vesicular impact melt matrix are obviously also fragments of QMG (see e.g., Figs. 5e–g). Comparing Fig. 5d and Figs. 5e–g, a difference in grain sizes between the large QMG clast LK10 and the smaller fragments can be observed. The grain size of minerals in the large QMG clast is below 100 μm, whereas some of the other QMG fragments show grain sizes of several hundred micrometers. However, the feldspar and pyroxene compositions are quite similar between QMG clasts or fragments, respectively (see Fig. 9). The plots in Fig. 9 show feldspar and pyroxene compositions for the QMG clast discussed above (LK10), compared to the QMG fragments and felsite clasts. Without investigating trace elements in situ, it cannot be concluded whether all the QMG and felsite fragments are from the same source rock or not.

### *High Mg# Pyroxene Clasts and a Single Pyroxenite Clast*

There is no hint that the abundant and relatively large monomineralic pyroxene clasts with a high Mg# are associated with any of the lithologies that we have characterized in the investigated thin sections. As no grain boundaries are discernible, their origin as fragments of pyroxenite can also be excluded. This observation makes their origin somewhat enigmatic. Measuring trace element concentrations of these high Mg# clasts may shed more light on their origin. In contrast, the single pyroxenite clast that we identified has a somewhat lower Mg# and comprises smaller individual pyroxene crystals (up to 150 μm in size). The lunar mantle is thought to consist of pyroxenite or dunite. For example, Ringwood and Essene (1970) proposed pyroxenite as a 200–500 km deep mantle source of mare basalts. A more recent study by Gagnepain-Beyneix et al. (2006) also found a pyroxenite mantle to be the best fit for the reevaluated seismic velocities of the Apollo seismic measurements. The Mg# of 79–80 of the pyroxenite clast is in good agreement with the values for the upper lunar mantle given in Wieczorek et al. (2006), and references therein. Nonetheless, pyroxenite clasts found in the lunar regolith are thought to most likely represent recrystallized pyroxene grains (Wilshire and Jackson 1972). Some pyroxenites in lunar regolith could also be relicts of impactors, for example, from nakhlite or aubrite achondrite meteorites. However, the clast discussed here has a typical lunar ratio of iron to manganese (see Fig. 2a), excluding a non-lunar origin.

### *Symplectite Clasts*

Comparable symplectitic assemblages are occasionally called "pyroxferroite breakdown material" or PBM in the literature (e.g., Warren et al. 2004). Such symplectite-like clasts are known from Apollo 11 samples (Chao et al. 1970) and also from some lunar meteorites, such as Asuka 881757 (Koeberl et al. 1993), NWA 773 (Fagan et al. 2003), and EET 96008 (Anand et al. 2003). Yet not all of them are thought to be the result of a pyroxferroite breakdown. Some authors argue that the bulk composition of the clasts is not consistent with pyroxferroite as a precursor phase. Synthetic pyroxferroite is stable only at pressures higher than 10 kbar (Lindsley and Burnham 1970). At lower pressure and a temperature of 960 °C, pyroxferroite decomposes within 68.5 h to the mineral assemblage Ca-rich clinopyroxene, fayalite, and tridymite (Lindsley et al. 1972). The bulk composition of the clasts discussed here ($En_{16.5}Fs_{68}Wo_{15.5}$) is outside the range reported for pyroxferroite with $En_{4–13}Fs_{75–82}Wo_{12–14}$ (Lindsley et al. 1972) and $En_{5–8}Fs_{70–81}Wo_{14–24}$ (Agrell et al. 1970). In addition, micro-Raman analysis revealed that the silica in the investigated clasts is quartz and not tridymite (see Fig. 3). However, it cannot be excluded that it formed as tridymite and was then inverted to quartz at a later time. Importantly, the texture of the studied symplectite-like clasts and other ones in the literature indicates extensive recrystallization of the mineral phases after formation of the symplectitic assemblage (Abart, personal communication).

### *Glasses*

With only a few exceptions, the various types of glasses present in NWA 11962 have relatively high Ti contents. The glassy impact melt matrix (Fig. 8f) of the meteorite has a $TiO_2$ concentration of 1.8 wt% (±0.5). Impact glass spherules have $TiO_2$ concentrations ranging from 1.3 to 9.8 wt%, whereas the volcanic glass spherules have $TiO_2$ concentrations from 3 to 8.5 wt%. The glass of the olivine vitrophyric fragments has a $TiO_2$ content of 5.1 wt% (±0.2) and the large opaque parts of the impact melt veins have an average composition of 5.7 wt% (±0.3). We compared the major element chemical compositions of the glass spherules listed in Table 2 with 25 groups of pristine

lunar glasses reported by Delano (1986). Glass spherules Sp10 and Sp0 have some similarities to Apollo 15 yellow glass, whereas glass spherules Sp2, Sp7, and Sp9 show a best fit with Apollo 17 orange glass. Glass spherule Sp4 has similarities with Apollo 14 yellow glass. However, in all cases, the iron content of the glass spherules in NWA 11962 is higher than in the respective Apollo glasses. It is possible that some of the black spherules are devitrified orange spherules, similar to the ones shown by Rutherford and Papale (2009). Unlike the glass spherules, the impact melt splashes have concentrations very similar to the glassy matrix of the meteorite (Table 3). Their shape and the fact that they bear small clasts at their rims (see Fig. S5) suggests that they were not completely solidified upon landing on the regolith and had a rather short flight time. For these reasons, we assume that they represent the composition of the regolith in the vicinity of the launch crater of NWA 11962.

## Composition of the Clasts and the Source Region

The classification of lunar mare basalts is based on their $TiO_2$ content (e.g., Giguere et al. 2000). The broadly used convention is that basalts with <1.5 wt% $TiO_2$ are defined as "very-low titanium" (VLT), basalts with 1.5–6 wt% $TiO_2$ as "low-Ti," and basalts with >6 wt% $TiO_2$ as "high-Ti" (Neal and Taylor 1992). Some authors have suggested different classification schemes. For example, Le Bas (2001) and later on Warren and Taylor (2014) have proposed that the classes as defined above should be denoted "Ti-poor," "medium-Ti," and "Ti-rich." Robinson et al. (2012) used the following categories: very-low Ti ($TiO_2$ <1%), low-Ti (1% < $TiO_2$ < 6%), intermediate-Ti (6–10% $TiO_2$), and high-Ti (>10% $TiO_2$), which is close to the initial classification of Papike and Vaniman (1978). However, as already noted by Warren and Taylor (2014), the use of "low-Ti" for basalts with up to 6 wt% $TiO_2$ is somehow strange, if not even misleading. Orbital remote sensing data have revealed that $TiO_2$ concentrations higher than 6 wt% are very rare on the lunar surface (Apollo 11 samples are an exception) and, therefore, the term intermediate may be misleading for such basalts. We, therefore, used the classification as proposed by Warren and Taylor (2014) in the following text.

Historically, the collections of Apollo and Luna basalt samples show a bimodal distribution with abundant Ti-poor (VLT) and Ti-rich (high-Ti) basalts and a low proportion of medium-Ti (low-Ti) basalts. However, the available collections are biased by a nonrandom sampling. Basalt clasts found in lunar meteorites, which represent a much larger and more random sampling of the lunar crust, as well as remote sensing data show that the distribution of basalts is in fact unimodal (Robinson et al. 2012), with much less Ti-rich basalts than Ti-poor and medium-Ti basalts. NWA 11962 represents a further example of the relative abundances of medium-Ti to Ti-rich basalts and, therefore, contributes to a better understanding of their global lunar distribution and, consequently, to a more accurate estimate of the composition of the lunar crust.

From their study of basalt clasts in lunar feldspathic meteorites, Robinson et al. (2012) concluded that the distribution of basalts in lunar meteorites is specific for the respective meteorite and, thus, constrains the source region to a certain point. In the case of NWA 11962, this means that the source region of this specific meteorite most likely lies in or a few hundred kilometers around the medium-Ti to Ti-rich regions found in Oceanus Procellarum and Mare Tranquillitatis. However, the mean chemical composition of the glassy matrix of NWA 11962 (see Table 3 and Fig. 6a) refers to a source regolith with approximately 1.8 wt% $TiO_2$. Regolith with a similar composition is widespread in many mare regions. However, our petrographic observations suggest that NWA 11962 is a binary mixture of material derived from mare and feldspathic highland terrane (FHT). In particular, it is a mixture of gabbroic basalt, vitrophyric glasses, and Mg- and alkali suite lithologies with minor amounts of (VHK) basalts, granulites, and impact breccias. Therefore, we estimate that the meteorite originated from a mare—highland mixing zone with a spatial proximity to medium-Ti and Ti-rich volcanic regions.

## Possible Pairing Relationships with Other Lunar Meteorites

Preliminary instrumental neutron activation analysis (INAA) on homogenized bulk powder revealed an Fe concentration of 9.28 wt% and a Th concentration of 6.6 ppm for NWA 11962 (Bechtold et al. 2020). Similar Fe and Th contents were reported in the literature for at least seven other lunar meteorites, suggesting a possible pairing relationship. Specifically, these are NWA 4472/4485 (Korotev et al. 2009), Miller Range 13317 (Curran et al. 2016), Calcalong Creek (Hill et al. 1991), Lynch 002 (Smith et al. 2012), Sayh al Uhaymir (SaU) 169 (Gnos et al. 2004), and Dhofar 1442 (Zeigler et al. 2011). We compare here their petrographic characteristics with those observed in NWA 11962, to support or exclude a possible pairing relationship.

### *NWA 4472/4485*

Of the seven lunar meteorites mentioned above, NWA 4472/4485 (paired stones) shows the closest match

in terms of bulk Fe and Th concentrations (Bechtold et al. 2020). In view of these similarities in Fe and Th concentrations, NWA 11962 and NWA 4472/4485 could be considered paired. Nonetheless, taking into account also the petrographic observations, these meteorites present some striking differences. Both meteorites were classified as lunar regolith breccias because they contain glass spherules. According to Joy et al. (2011), in the case of NWA 4472, all glass spherules are of impact origin. As discussed above, in the case of NWA 11962, approximately half of the spherules are of volcanic origin. Besides this, Joy et al. (2011) report that all impact glasses in NWA 4472 have less than 4.5 wt% $TiO_2$, indicating that no high-Ti basalt bedrock was melted. As can be seen from Table 2 and Fig. 6a, many of the glass spherules in NWA 11962 have higher $TiO_2$ contents than 4.5 wt%, disregarding their impact or volcanic origin. Arai et al. (2009) reported glass spherules in NWA 4485 having 1.2–1.8 wt% $TiO_2$. Additionally, on a plot of Ti# (Ti/[Ti + Cr]) versus Fe# (Fe/[Fe + Mg]) pyroxenes from NWA 11962 plot in the field of low to high titanium (LT and HT), whereas the pyroxenes from NWA 4472 plot in the very low to low titanium (VLT and LT) region (see Fig. 6b). The different Ti concentrations in glass spherules, as well as in pyroxenes, suggest a different origin for the volcanic products in the source crater regolith of NWA 11962 compared to NWA 4485/4472. Furthermore, in contrast to the basalt clasts of NWA 4472, none but one of the studied basaltic clasts in NWA 11962 contains olivine. This olivine is Fe-rich ($Fa_{47.5}$). In contrast, the olivine of the basalts in NWA 4472 is substantially more Mg-rich ($Fa_{39–54}$). The plagioclase compositions are considerably more anorthitic (Ca-rich) in the basalts of NWA 11962 compared to NWA 4472. Both meteorites contain felsite clasts in the form of granophyric intergrowth of K-feldspar and silica. The K-feldspar compositions of the granophyric intergrowths are almost congruent, with $Or_{63–83}Ab_{13–30}Cn_{2.8–6.5}$ for NWA 11962 and $Or_{56–81}Ab_{15–30}Cn_{0.6–6.3}$ for NWA 4472 (Kuehner et al. 2007). However, they are comparable to values from Apollo samples in the literature, for example, $Or_{67.8}Ab_{28.2}An_{4.0}$ (average for K-feldspar in 12033,507), $Or_{33–78}Ab_{21–50}An_{0.7–16}Cn_{0.4–3.9}$ (in 12032,366-19), and $Or_{83}Ab_{12}An_{1.7}Cn_{3.5}$ (average for K-feldspar in 14161,7373). The abundant monomineralic high-Mg, low-Ca pyroxene grains (see Fig. 4b), presumably from an Mg-suite rock, present in NWA 11962, are lacking in NWA 4472. To our knowledge, NWA 11962 contains no Mg-suite breccias, harzburgite, spinel troctolite, granulite, or norite clasts as does NWA 4472. The majority of these petrographic observations are arguments against a pairing relation. However, the representativeness of the small meteorite fragment investigated in this work compared to the whole mass of the meteorite cannot be ignored, especially considering that NWA 11962 is a breccia. Measuring and comparing cosmic ray exposure (CRE) ages (Eugster 2003) and terrestrial ages (Jull 2001) would provide additional information to discuss possible pairing relations.

### *Miller Range 13317*

Miller Range 13317 is a basaltic regolith breccia, with a VLT basalt component (Zeigler and Korotev 2016a). According to Curran et al. (2016), the clasts in the breccia include regolith breccias, basalts, feldspathic fragments, symplectites, norites, and granulites. The same authors reported an FeO concentration of 9–16 wt% (Fe = 6.99–12.43 wt%) and a Th concentration of 5.4 ppm, which is comparable to NWA 11962. Yet, no quartz monzogabbros, lunar felsite clasts, or olivine vitrophyric glasses have been reported in petrographic descriptions for Miller Range 13317 in the literature (Curran et al. 2016, 2019; Zeigler and Korotev 2016a, 2016b). This fact and the VLT basalt component in MIL 13317 (compare Fig. 4b in Curran et al. 2019 and Fig. 6b in this study) make a pairing relation to NWA 11962 rather unlikely.

### *Calcalong Creek*

This lunar meteorite has been described as a polymict breccia with clasts of mare and highland origin (Hill and Boynton 2003). Calcalong Creek has a bulk FeO concentration of 9.69 wt% (Fe = 7.53 wt%) (Hill and Boynton 2003) or 9.66 wt% (Korotev et al. 2009) and a Th concentration of 4.28 ppm (Hill and Boynton 2003) or 3.95 ppm (Korotev et al. 2009). These values are similar to the values of Fe and Th found in NWA 11962 (Bechtold et al. 2020). However, the clast inventory of Calcalong Creek is significantly different to what we report here for NWA 11962. Although it contains one clast with a KREEPy signature, it has no K-feldspar and only a few small silica clasts. No quartz monzogabbro, lunar felsite clasts, or vitrophyric glasses have been reported for this meteorite. Furthermore, the basalts in Calcalong Creek all carry a low-Ti to very-low-Ti signature. With regard to the low-Ti to high-Ti pyroxenes and spherules in NWA 11962, this makes a pairing relation rather unlikely.

### *Lynch 002*

Korotev (2013) reported an FeO concentration of 9.0 (±0.3) wt% (Fe = 6.99 wt%) and a Th concentration of 5.1 (±1.2) ppm for this lunar meteorite, values that are quite similar to those for NWA 11962. The petrographic description for this lunar meteorite is limited to two conference abstracts (Smith et al. 2012; Robinson et al. 2016). No quartz monzogabbro, lunar felsite, gabbroic

clasts, or olivine vitrophyric glasses have been reported therein. Robinson et al. (2016) described several basalt clasts, with pyroxene compositions indicating a heritage from low-Ti to very-low-Ti parent magmas. The sum of these petrographic observations makes a pairing relation to NWA 11962 very unlikely.

### *Sayh al Uhaymir 169*

SaU 169 consists of two different parts, namely a KREEP-rich impact melt breccia and a KREEP-rich regolith. Gnos et al. (2004) reported that the impact melt breccia part has a very high Th concentration (32.7 ppm), which is nearly five times the Th concentration in NWA 11962. However, the same authors reported that the regolith part of this lunar meteorite has an FeO concentration of 11.09 wt% (Fe = 8.62 wt%) and a Th concentration of 8.44 ppm, which is just slightly higher than in NWA 11962. According to Gnos et al. (2004), the regolith breccia part of SaU 169 contains basalt clasts with a full range from low-Ti to high-Ti basalts as well as orange glass beads for which no composition is available. Beside this, no monzogabbro, neither lunar felsite clasts, nor olivine vitrophyric glasses have been described in SaU 169 by Gnos et al. (2004). Based on the limited amount of petrographic information available for SaU 169, it is impossible to either confirm or exclude a pairing relationship with NWA 11962.

### *Dhofar 1442*

Dhofar 1442 has been described as a clast-rich regolith breccia with a glassy melt matrix (Zeigler et al. 2011). It has an Fe concentration of 13.56 wt% (Fe = 10.54 wt%) and a Th concentration of 14.4 ppm. Despite the higher Fe and Th concentrations compared to NWA 11962, the mineral and lithic clast inventory is very similar. Zeigler et al. (2011) reported that the impact-related glasses in Dhofar 1442 typically have compositions related to the bulk composition of the meteorite. We also observed this in NWA 11962 for the glassy clasts denoted and discussed as impact melt splashes above. A comparison of the data and figures in Zeigler et al. (2011) and in Demidova et al. (2014) with our results shows that the mineral chemistry and the texture of many of the clasts in Dhofar 1442 are very similar to clasts in NWA 11962. Despite the differences in bulk FeO and Th concentrations, this is the most interesting lunar meteorite in terms of a possible pairing relation to NWA 11962 (in addition to NWA 4472/4485). Interestingly, Demidova et al. (2014) noted that the age variation of zircons in Dhofar 1442 is comparable to the age variation of zircons in NWA 4485. However, Ti-rich glasses and olivine vitrophyric glass appear to be less common in Dhofar 1442 than in NWA 11962.

## CONCLUSIONS

NWA 11962 is a lunar meteorite classified as a lunar regolith breccia. The lunar origin of the meteorite has been confirmed by oxygen isotopes and mineral chemistry. It contains clasts from various lunar lithologies, including the alkali suite which is rare in the Apollo collection, magnesian suite, and mare (or VHK) basalts. The investigated sample additionally shows a glassy matrix of vesicular impact melt and abundant gabbroic clasts that both occupy large areas in the investigated thin sections. The mineral chemistry of pyroxene and the major element chemistry of the various glasses in NWA 11962 show that the meteorite has inherited certain materials produced during lunar medium-Ti to Ti-rich volcanism. In summary, NWA 11962 is a binary mixture of mare and feldspathic highland terrane materials that most likely originated from such a mixing zone with nearby medium-Ti to Ti-rich regions on the lunar near side. Seven other lunar meteorites (as discussed above) have comparable bulk FeO and Th concentrations to NWA 11962, with at least two of them, NWA 4472/4485 and Dhofar 1442, showing certain similarities that might be consistent with a possible pairing relationship. However, as the meteorites considered here have only been compared based on information available in the literature, no firm conclusions can be drawn. Measuring and comparing cosmic ray exposure (CRE) ages (Eugster 2003) and terrestrial ages (Jull 2001) would provide additional information to discuss possible pairing relations.

*Acknowledgments*—We thank Dan Topa (NHM Vienna) and Franz Kiraly (University of Vienna) for assistance with EPMA analyses, Eugen Libowitzky (University of Vienna) for assistance with the micro-Raman spectroscopic analyses, and Goran Batic (NHM Vienna) for sample preparation. The investigated thin sections were kindly provided by the NHM Vienna. Oxygen isotope studies at the Open University are funded by a consolidated grant from the Science and Technology Facilities Council (STFC), UK GRANT NUMBER: ST/T000228/1. We are grateful to Randy L. Korotev and an anonymous reviewer for constructive reviews and to A. J. Timothy Jull for efficient editorial handling.

*Data Availability Statement*—The data that support the findings of this study are available from the corresponding author upon reasonable request.

*Editorial Handling*—Dr. A. J. Timothy Jull

## REFERENCES


Agrell S., Scoon J., Muir I., Long J., McConnell J., and Peckett A. 1970. Observations on the chemistry, mineralogy and petrology of some Apollo 11 lunar samples. In *Proceedings of the Apollo 11 Lunar Science Conference. Volume 1: Mineralogy and Petrology*, edited by Levinson A. A. New York: Pergamon Press. pp. 93–128.

Anand M., Taylor L. A., Neal C. R., Snyder G. A., Patchen A., Sano Y., and Terada K. 2003. Petrogenesis of lunar meteorite EET 96008. *Geochimica et Cosmochimica Acta* 67:3499–3518.

Arai T., Misawa K., Tomiyama T., Yoshitake M., and Irving A. J. 2009. Constraints on lunar KREEP magmatism: A variety of KREEP basalt derivatives in lunar meteorite NWA 4485 (abstract #2292). 40th Lunar and Planetary Science Conference. CD-ROM.

Bechtold A., Koeberl C., Brandstätter F., and Greenwood R. 2020. NWA 11962: A new lunar meteorite and its presumed source region in the Procellarum KREEP terrane (abstract). European Lunar Symposium 2020, 12–14 May 2020, Virtual, 2 pp. https://els2020.arc.nasa.gov/abstracts.

Brandstätter F., Koeberl C., and Kurat G. 1991. The discovery of iron barringerite in lunar meteorite Y-793274. *Geochimica et Cosmochimica Acta* 55:1173–1174.

Chao E. C. T., Minkin J. A., Frondel C., Klein Jr. C., Drake J. C., Fuchs L., Tani B., Smith J. V., Anderson A. T., Moore P. B., Zechman Jr. G. R., Traill R. J., Plant A. G., Douglas J. A. V., and Dence M. R. 1970. Pyroxferroite, a new calcium-bearing iron silicate from Tranquillity Base. In *Proceedings of the Apollo 11 Lunar Science Conference. Volume 1: Mineralogy and Petrology*, edited by Levinson A. A. New York: Pergamon Press. pp. 65–79.

Cohen B. A., James O. B., Taylor L. A., Nazarov M. A., and Barsukova L. D. 2004. Lunar highland meteorite Dhofar 026 and Apollo sample 15418: Two strongly shocked, partially melted, granulitic breccias. *Meteoritics & Planetary Science* 39:1419–1447.

Collareta A., D'Orazio M., Gemelli M., Pack A., and Folco L. 2016. High crustal diversity preserved in the lunar meteorite Mount DeWitt 12007 (Victoria Land, Antarctica). *Meteoritics & Planetary Science* 51:351–371.

Curran N., Joy K., Pernet-Fisher J., and Burgess R. 2016. A new basaltic-bearing lunar meteorite Miller Range 13317 (abstract #1516). 47th Lunar and Planetary Science Conference. CD-ROM.

Curran N. M., Joy K. H., Snape J. F., Pernet-Fisher J. F., Gilmour J. D., Nemchin A. A., Whitehouse M. J., and Burgess R. 2019. The early geological history of the Moon inferred from ancient lunar meteorite Miller Range 13317. *Meteoritics & Planetary Science* 54:1401–1430.

Day J. M. and Taylor L. A. 2007. On the structure of mare basalt lava flows from textural analysis of the LaPaz Icefield and Northwest Africa 032 lunar meteorites. *Meteoritics & Planetary Science* 42:3–17.

Day J. M., Taylor L. A., Floss C., Patchen A. D., Schnare D. W., and Pearson D. G. 2006. Comparative petrology, geochemistry, and petrogenesis of evolved, low-Ti lunar mare basalt meteorites from the LaPaz Icefield, Antarctica. *Geochimica et Cosmochimica Acta* 70:1581–1600.

Delano J. W. 1986. Pristine lunar glasses: Criteria, data, and implications. *Journal of Geophysical Research: Solid Earth* 91:201–213.

Delano J. and Livi K. 1981. Lunar volcanic glasses and their constraints on mare petrogenesis. *Geochimica et Cosmochimica Acta* 45:2137–2149.

Demidova S. I., Nazarov M. A., Anosova M. O., Kostitsyn Y. A., Ntaflos T., and Brandstätter F. 2014. U-Pb zircon dating of the lunar meteorite Dhofar 1442. *Petrology* 22:1–16.

Eugster O. 2003. Cosmic-ray exposure ages of meteorites and lunar rocks and their significance. *Chemie der Erde-Geochemistry* 63:3–30.

Fagan T. J., Taylor G. J., Keil K., Hicks T. l., Killgore M., Bunch T. E., Wittke J. H., Mittlefehldt D. W., Clayton R. N., Mayeda T. K., Eugster O., Lorenzetti S., and Norman M. D. 2003. Northwest Africa 773: Lunar origin and iron-enrichment trend. *Meteoritics & Planetary Science* 38:529–554.

Fagan T. J., Kashima D., Wakabayashi Y., and Suginohara A. 2014. Case study of magmatic differentiation trends on the Moon based on lunar meteorite Northwest Africa 773 and comparison with Apollo 15 quartz monzodiorite. *Geochimica et Cosmochimica Acta* 133:97–127.

Gagnepain-Beyneix J., Lognonné P., Chenet H., Lombardi D., and Spohn T. 2006. A seismic model of the lunar mantle and constraints on temperature and mineralogy. *Physics of the Earth and Planetary Interiors* 159:140–166.

Giguere T. A., Taylor G. J., Hawke B. R., and Lucey P. G. 2000. The titanium content of lunar mare basalts. *Meteoritics & PIanetary Science* 35:193–200.

Gnos E., Hofmann B. A., Al-Kathiri A., Lorenzetti S., Eugster O., Whitehouse M. J., Villa I. M., Jull A. J. T., Eikenberg J., Spettel B., Krähenbühl U., Franchi I. A., and Greenwood R. C. 2004. Pinpointing the source of a lunar meteorite: Implications for the evolution of the Moon. *Science* 305:657–659.

Greenwood R. C., Barrat J.-A., Yamaguchi A., Franchi I. A., Scott E. R., Bottke W. F., and Gibson J. M. 2014. The oxygen isotope composition of diogenites: Evidence for early global melting on a single, compositionally diverse, HED parent body. *Earth and Planetary Science Letters* 390:165–174.

Greenwood R. C., Burbine T. H., Miller M. F. I. A., and Franchi I. A. 2017. Melting and differentiation of early-formed asteroids: The perspective from high precision oxygen isotope studies. *Chemie der Erde-Geochemistry* 77:1–43.

Gross J., Treiman A. H., and Mercer C. N. 2014. Lunar feldspathic meteorites: Constraints on the geology of the lunar highlands, and the origin of the lunar crust. *Earth and Planetary Science Letters* 388:318–328.

Harper M. 2020. python-ternary: Ternary plots in Python. Version 1.0.6. https://10.5281/zenodo.594435

Hidaka Y., Yamaguchi A., and Ebihara M. 2014. Lunar meteorite, Dhofar 1428: Feldspathic breccia containing KREEP and meteoritic components. *Meteoritics & Planetary Science* 49:921–928.

Hill D. H. and Boynton W. V. 2003. Chemistry of the Calcalong Creek lunar meteorite and its relationship to lunar terranes. *Meteoritics & Planetary Science* 38:595–626.

Hill D. H., Boynton W. V., and Haag R. A. 1991. A lunar meteorite found outside the Antarctic. *Nature* 352:614.

Jolliff B., Floss C., McCallum I., and Schwartz J. 1999. Geochemistry, petrology, and cooling history of 14161, 7373: A plutonic lunar sample with textural evidence of

granitic-fraction separation by silicate-liquid immiscibility. *American Mineralogist* 84:821–837.

Joy K. H. and Arai T. 2013. Lunar meteorites: New insights into the geological history of the Moon. *Astronomy & Geophysics* 54:4–28.

Joy K., Burgess R., Hinton R., Fernandes V., Crawford I., Kearsley A., Irving A., and the Edinburgh Ion Microprobe Facility. 2011. Petrogenesis and chronology of lunar meteorite Northwest Africa 4472: A KREEPy regolith breccia from the Moon. *Geochimica et Cosmochimica Acta* 75:2420–2452.

Jull A. T. 2001. Terrestrial ages of meteorites. In *Accretion of extraterrestrial matter throughout Earth's history*, edited by Peucker-Ehrenbrink B. and Schmitz B. New York: Springer. pp. 241–266.

Karner J., Papike J., and Shearer C. 2006. Comparative planetary mineralogy: Pyroxene major-and minor-element chemistry and partitioning of vanadium between pyroxene and melt in planetary basalts. *American Mineralogist* 91:1574–1582.

Koeberl C., Kurat G., and Brandstätter F. 1993. Gabbroic lunar mare meteorites Asuka-881757 (Asuka-31) and Yamato-793169: Geochemical and mineralogical study. *Proceedings of the NIPR Symposium on Antarctic Meteorites* 6:14–34.

Korotev R. L. 2005. Lunar geochemistry as told by lunar meteorites. *Chemie der Erde-Geochemistry* 65:297–346.

Korotev R. L. 2013. Composition of Lynch 002 lunar meteorite (abstract #5021). *Meteoritics & Planetary Science* 48.

Korotev R. L., Zeigler R. A., Jolliff B. L., Irving A. J., and Bunch T. E. 2009. Compositional and lithological diversity among brecciated lunar meteorites of intermediate iron concentration. *Meteoritics & Planetary Science* 44:1287–1322.

Korotev R. L. and Irving A. J. 2021. Lunar meteorites from northern Africa. *Meteoritics & Planetary Science* 56:206–240.

Kuehner S., Irving A., Korotev R., Hupé G., and Ralew S. 2007. Zircon-baddeleyite-bearing silica+ K-feldspar granophyric clasts in KREEP-rich lunar breccias Northwest Africa 4472 and 4485 (abstract# 1516). 38th Lunar and Planetary Science Conference. CD-ROM.

Lafuente B., Downs R. T., Yang H., and Stone N. 2015. The power of databases: The RRUFF project. In *Highlights in mineralogical crystallography*, edited by Armbruster T. and Danisi R. M. Berlin: De Gruyter. pp. 1–30.

Le Bas M. L. 2001. Report of the working party on the classification of the lunar igneous rocks. *Meteoritics & Planetary Science* 36:1183–1188.

Lindsley D. H. and Burnham C. W. 1970. Pyroxferroite: Stability and X-ray crystallography of synthetic $Ca_{0.15}Fe_{0.85}SiO_3$ pyroxenoid. *Science* 168:364–367.

Lindsley D., Papike J., and Bence A. 1972. Pyroxferroite: Breakdown at low pressure and high temperature (abstract). 3rd Lunar Science Conference. p. 483.

McKay D. S., Heiken G., Basu A., Blanford G., Simon S., Reedy R., French B. M., and Papike J. 1991. The lunar regolith. In *Lunar sourcebook*, edited by Heiken G. H., Vaniman D. T., and French B. M. Cambridge: Cambridge University Press. pp. 285–356.

Miller M. F. 2002. Isotopic fractionation and the quantification of $^{17}O$ anomalies in the three oxygen isotope system: An appraisal and geochemical significance. *Geochimica et Cosmochimica Acta* 66:1881–1889.

Neal C. R. 2009. The Moon 35 years after Apollo: What's left to learn?. *Geochemistry* 69:3–43.

Neal C. R. and Taylor L. A. 1992. Petrogenesis of mare basalts: A record of lunar volcanism. *Geochimica et Cosmochimica Acta* 56:2177–2211.

Neal C., Taylor L., Schmitt R., Hughes S., and Lindstrom M. 1989. High alumina (HA) and very high potassium (VHK) basalt clasts from Apollo 14 breccias. II-Whole rock geochemistry-Further evidence for combined assimilation and fractional crystallization within the lunar crust. Proceedings, 19th Lunar and Planetary Science Conference. pp. 147–161.

Nielsen R. and Drake M. 1978. The case for at least three mare basalt magmas at the Luna 24 landing site. In *Mare Crisium: The view from Luna 24*, edited by Merrill R. B. and Papike J. J. New York: Pergamon Press, Inc. pp. 419–428.

Papike J. J. and Vaniman D. T. 1978. Luna 24 ferrobasalts and the mare basalt suite—Comparative chemistry, mineralogy, and petrology. In *Mare Crisium: The view from Luna 24*, edited by Merrill R. B. and Papike J. J. New York: Pergamon Press. pp. 371–401.

Papike J., Taylor L., and Simon S. 1991. Lunar minerals. In *Lunar sourcebook*, edited by Heiken G. H., Vaniman D. T., and French B. M. Cambridge: Cambridge University Press. pp. 121–182.

Papike J., Ryder G., and Shearer Jr. C. 1998. Lunar samples. In *Planetary materials*, edited by Papike J. Reviews in Mineralogy and Geochemistry, 36. Washington, D.C.: American Mineralogical Society. pp. 1–234.

Papike J., Karner J., and Shearer C. 2003. Determination of planetary basalt parentage: A simple technique using the electron microprobe. *American Mineralogist* 88:469–472.

Papike J., Karner J., Shearer C., and Burger P. 2009. Silicate mineralogy of martian meteorites. *Geochimica et Cosmochimica Acta* 73:7443–7485.

Ringwood A. and Essene E. 1970. Petrogenesis of Apollo 11 basalts, internal constitution and origin of the Moon. Proceedings of the Apollo 11 Lunar Science Conference. pp. 769–799.

Robinson K. and Taylor G. 2011. Intrusive and extrusive lunar felsites (abstract #1257). 42nd Lunar and Planetary Science Conference. CD-ROM.

Robinson K. L., Smith C. L., Kearsley A. T., Bevan A. W. R., and Anand M. 2016. The Lynch 002 lunar meteorite revisited (abstract #1470). 47th Lunar and Planetary Science Conference. CD-ROM.

Robinson K. L., Treiman A. H., and Joy K. H. 2012. Basaltic fragments in lunar feldspathic meteorites: Connecting sample analyses to orbital remote sensing. *Meteoritics & Planetary Science* 47:387–399.

Roduit N. J. 2020. MicroVision: Image analysis toolbox for measuring and quantifying components of high-definition images. Version 1.3.1.

Rutherford M. J. and Papale P. 2009. Origin of basalt fire-fountain eruptions on Earth versus the Moon. *Geology* 37:219–222.

Rutherford M. J., Head J. W., Saal A. E., Hauri E., and Wilson L. 2017. Model for the origin, ascent, and eruption of lunar picritic magmas. *American Mineralogist* 102:2045–2053.

Ryder G., Stoeser D. B., Marvin U. B., and Bower J. 1975. Lunar granites with unique ternary feldspars. Proceedings, 6th Lunar Science Conference. pp. 435–449.

Seddio S. M., Korotev R. L., Jolliff B., and Wang A. 2015. Silica polymorphs in lunar granite: Implications for granite petrogenesis on the Moon. *American Mineralogist* 100:1533–1543.

Shervais J. W., Taylor L. A., and Laul J. 1983. Ancient crustal components in the Fra Mauro breccias (abstract). 14th Lunar and Planetary Science Conference. *Journal of Geophysical Research, Supplement* 88:B177–B192.

Shervais J., Taylor L., and Laul J. 1984. Very high potassium (VHK) basalt: A new type of aluminous mare basalt from Apollo 14 (abstract). 15th Lunar and Planetary Science Conference. p. 768.

Shervais J. W., Taylor L. A., and Lindstrom M. M. 1985. Apollo 14 mare basalts: Petrology and geochemistry of clasts from consortium breccia 14321. *Journal of Geophysical Research: Solid Earth* 90:C375–C395.

Smith C., Kearsley A., Bermingham K., Deacon G., Kurahashi E., Franchi I., and Bevan A. 2012. Lynch 002: A new lunar meteorite from the Nullarbor Desert, Western Australia (abstract #5137). *Meteoritics & Planetary Science* 75.

Stephant A., Anand M., Ashcroft H. O., Zhao X., Hu S., Korotev R. L., Strekopytov S., Greenwood R. C., Humphreys-Williams E., Liu Y., Tang G., Li Q., and Franchi I. A. 2019. An ancient reservoir of volatiles in the Moon sampled by lunar meteorite Northwest Africa 10989. *Geochimica et Cosmochimica Acta* 266:163–183.

Stöffler D., Ryder G., Ivanov B. A., Artemieva N. A., Cintala M. J., and Grieve R. A. 2006. Cratering history and lunar chronology. In *New views of the Moon*, edited by Jolliff B. L., Wieczorek M. A., Shearer C. K., and Neal C. R. Reviews in Mineralogy and Geochemistry Reviews in mineralogy and geochemistry, 60. Washington, D.C.: Mineralogical Society of America. pp. 519–596.

Valencia S. N., Jolliff B. L., and Korotev R. L. 2019. Petrography, relationships, and petrogenesis of the gabbroic lithologies in Northwest Africa 773 clan members Northwest Africa 773, 2727, 3160, 3170, 7007, and 10656. *Meteoritics & Planetary Science* 54:2083–2115.

Warren P. H. 1998. A brief review of the scientific importance of lunar meteorites. In *Workshop on New Views of the Moon: Integrated Remotely Sensed, Geophysical, and Sample Datasets*, edited by Jolliff B. L. and Ryder G. Houston, Texas: Lunar and Planetary Institute. 74 p.

Warren P. H. 2005. "New" lunar meteorites: Implications for composition of the global lunar surface, lunar crust, and the bulk Moon. *Meteoritics & Planetary Science* 40:477–506.

Warren P. H. and Taylor G. J. 2014. The Moon. In *Treatise on geochemistry*, 2nd ed., edited by Holland H. D. and Turekian K. K. Oxford: Elsevier. pp. 213–250.

Warren P. H., Greenwood J. P., and Rubin A. E. 2004. Los Angeles: A tale of two stones. *Meteoritics & Planetary Science* 39:137–156.

Warren P. H., Ulff-møller F., and Kallemeyn G. W. 2005. "New" lunar meteorites: Impact melt and regolith breccias and large-scale heterogeneities of the upper lunar crust. *Meteoritics & Planetary Science* 40:989–1014.

Wieczorek M., Jolliff B., Khan A., Pritchard M., Weiss B., Williams J., Hood L., Righter K., Neal C., Shearer C., McCallum I., Tompkins S., Hawke B., Peterson C., Gillis J., and Bussey B. 2006. The constitution and structure of martian meteorites. In *New views of the Moon*, edited by Jolliff B. L., Wieczorek M. A., Shearer C. K., and Neal C. R. Reviews in mineralogy and geochemistry, 60. Washington, D.C.: Mineralogical Society of America. pp. 221–364.

Wilshire H. and Jackson E. 1972. Lunar "dunite", "pyroxenite" and "anorthosite". *Earth and Planetary Science Letters* 16:396–400.

Zeigler R., Korotev R., and Jolliff B. 2011. Petrography and geochemistry of lunar meteorite Dhofar 1442 (abstract #1012). 42nd Lunar and Planetary Science Conference. CD-ROM.

Zeigler R. A. and Korotev R. L. 2016a. Petrography and geochemistry of lunar meteorite Miller Range 13317 (abstract #2554). 47th Lunar and Planetary Science Conference. CD-ROM.

Zeigler R. A. and Korotev R. L. 2016b. Petrography, geochemistry, and pairing relationships of basaltic lunar meteorite Miller Range 13317 (abstract #6257). *Meteoritics & Planetary Science* 51.

## SUPPORTING INFORMATION

Additional supporting information may be found in the online version of this article.

**Fig. S1**. Backscattered electron (BSE) image of a recrystallized impact melt globule with intersertal texture and abundant mafic minerals.

**Fig. S2**. BSE images of high-Mg# pyroxene clasts scattered throughout the matrix of NWA 11962.

**Fig. S3**. Pyroxenite clast in NWA 11962. a) BSE image. b) In plane-polarized light. c) Crossed polarizers. d) Detail showing exsolution lamellae under crossed polarizers. Note the various opaque inclusions.

**Fig. S4**. BSE images of glass spherules scattered throughout the matrix of the regolith breccia NWA 11962. Spherules of both volcanic and impact origin occur (see corresponding section in the main text).

**Fig. S5**. BSE images of glassy impact melt splashes in the matrix of NWA 11962.

**Fig. S6**. Example of an impact breccia as can be found in thin section NHMV-O266. The clasts in the breccia are similar to the clasts in the meteorite.

**Fig. S7**. Example of a granulite clast in thin section NHMV-O266.

**Table S1**. Electron microprobe detection limits.

**Table S2**. Petrographic overview of the clast content in NWA 11962.